Weierstraß-Institut
für Angewandte Analysis und Stochastik

Leibniz-Institut im Forschungsverbund Berlin e. V.

Preprint ISSN 2198-5855

A poro-visco-elastodynamic model in Eulerian formulation, its analysis, implementation, and application to phase transitions in the hydrated Earth's mantle

Dirk Peschka[1], Tomáš Roubíček[2,3]

submitted: January 28, 2026

[1] Weierstrass Institute
Anton-Wilhelm-Amo. 39
10117 Berlin
Germany
E-Mail: dirk.peschka@wias-berlin.de

[2] Charles University
Mathematical Institute
Sokolovská 83
186 75 Praha 8
Czech Republic
E-Mail: tomas.roubicek@mff.cuni.cz

[3] Czech Academy of Sciences
Institute of Thermomechanics
Dolejškova 5
182 00 Praha 8
Czech Republic

No. 3258
Berlin 2026

2020 *Mathematics Subject Classification.* 76N06, 35Q86, 86A99, 74F10, 65M60.

Key words and phrases. Heterogenous compressible continua, geophysical mantle dehydration and 660-km discontinuity, weak solutions and numerics.

The authors are very thankful to Marita Thomas for many valuable remarks and suggestions. D.P. thanks for the funding within the DFG Priority Program SPP 2171 Dynamic Wetting of Flexible, Adaptive, and Switchable Surfaces, project #422792530. T.R. acknowledges hospitality of the Weierstrass Institute Berlin and also a support from the CSF (Czech Science Foundation) project no. 23-06220S and the institutional support RVO: 61388998 (ČR).

Edited by
Weierstraß-Institut für Angewandte Analysis und Stochastik (WIAS)
Leibniz-Institut im Forschungsverbund Berlin e. V.
Anton-Wilhelm-Amo-Straße 39
10117 Berlin
Germany

Fax: +49 30 20372-303
E-Mail: preprint@wias-berlin.de
World Wide Web: http://www.wias-berlin.de/

A poro-visco-elastodynamic model in Eulerian formulation, its analysis, implementation, and application to phase transitions in the hydrated Earth's mantle

Dirk Peschka, Tomáš Roubíček

Abstract

A rather general-purpose poro-visco-elastodynamic model for compressible porous-like media at finite strains in Eulerian formulation in a prescribed gravitational field is studied. The mathematical analysis of the existence of weak solutions is based on a fully-implicit regularized time discretization, which is shown to be numerically stable for sufficiently small time steps and, in a multipolar variant, convergent in terms of subsequences. Applications to geophysical modelling of dehydration of descending wetted slabs or ascending plumes undergoing a volumetric phase transition at the interface between the upper and the lower mantle at 660 km depth, based on a barotropic viscoelastic fluid, are outlined. Implementation aspects via a standard finite element approach are outlined and some 2D computational experiments that highlight some aspects of this compressible geophysical model are presented.

1 Introduction

Eulerian formulations of continuum mechanics are a fundamental framework for modelling mechanical and thermomechanical systems and have become classics in many textbooks, *e.g.* [16, 22]. A particularly important class of problems are concerned with flowing or deforming materials that involve the transport of additional (fluidic) components by flow or diffusion [4]. Such kind of models have numerous applications, ranging from biomechanical descriptions of hydrogels, geological formations of porous soil and rocks in the Earth's crust as in the petroleum industry or during land slides or CO_2-storage or hydraulic fracturing, or hydrated rock dynamics in the deep Earth's mantle.

An advantage of a Eulerian formulation, *i.e.*, formulating the evolution laws in the actual evolving configuration instead of a static referential configuration, and of a corresponding Eulerian numerical implementation is that it reveals the "actual physics". For example, it employs the Cauchy stress instead of the Piola-Kirchhoff stress or it does not require re-meshing of the space discretization even under large displacements during long time evolution. On the other hand, it usually requires a fixed domain to circumvent cumbersome analytical technicalities and nonlinearities that are created by treating free boundary problems. For evolving domains, this drawback can be partially overcome by surrounding the moving domain of interest by some soft material (like air) and by embedding it into some larger fixed domain, which in geoscience is called a *sticky air* approach [10] or in the engineering community is called a fictitious-domain approach or an immersed-boundary method.

The treatment of earth by a compressible model allows for a proper modelling based on a *state equation* relating mass density and pressure and avoiding the necessity of various approximations that otherwise would be needed in incompressible models in anisothermal situations, such as the Boussinesq or the so-called anelastic liquid approximation, cf. [18], to capture buoyancy in a gravity field.

The goal of this paper is to demonstrate that the fully compressible model can well describe buoyancy in a gravity field and even some phase transformations. Having in mind the Earth's mantle dynamics as one of possible applications, we demonstrate that our compressible model can be used for numerical simulations both of descending slabs and also of ascending plumes moving upward through lower mantle and possibly interacting with the 660 km discontinuity even in the isothermal case. It should be emphasized that these phenomena are usually modelled isothermally, either compressible or, more conventionally, by using incompressible models with

DOI 10.20347/WIAS.PREPRINT.3258 Berlin 2026

the Boussinesq buoyancy approximation or the aforementioned anelastic fluid approximation, and rely on a very high Prandtl number ($\sim 10^{25}$ in the Earth's mantle), cf. *e.g.* [13, 18, 20, 35].

Having in mind rather specific applications to planetary modelling, we focus on *compressible barotropic fluids*. Thus, except Remark 2.3, we ignore shear elastic response and thus confine ourselves to a fluidic type model. In the Eulerian description, we thus consider the fluidic compressible Navier-Stokes rheology combined with the diffusion of a fluid content. The fluid content, which we call *diffusant*, is considered an extensive variable and its transport is driven by the gradient of the chemical potential. In particular, this allows the coupling of conventional Biot type poroelastic model to mechanics and diffusion. Nevertheless, we confine this study to isothermal situations, which limits the direct applicability of the model and rather demonstrates the usefulness of the compressible approach. Furthermore, we implement a sticky air by means of a specific scalar-valued composition field denoted by χ below. Such a composition field χ can be used to model the heterogeneity due to the air-solid interface but also to describe crust-mantle features, the latter being used in [2]. This methodology is similar to the reference map approach with indicator functions to incorporate heterogeneities used in [27]. We also discuss the analysis of the model using time-discretization and also consider various variants of the models such as Kelvin-Voigt or the anti-Zener (also called Jeffreys) rheologies, cf. Remark 2.3 and the time-discretization of the mere visco-elastodynamic part in [31].

The plan of the paper is the following. In Section 2, we formulate the isothermal poro-visco-elastodynamic model in the Eulerian frame in a prescribed gravitation field and study its energetics. In Section 3, we then analyse this model by the implicit time discretization, which also suggests a conceptual computational strategy. In particular, a-priori estimates and convergence (in the sense of subsequences) to suitably formulated weak solutions is proved there. Then, in Section 4, we illustrate the quasistatic variant of this compressible model on the specific geophysical applications, namely on the Earth's mantle dynamics where the rocky medium underwent volumetric phase transitions on specific pressures. A particular (and the main) transition in the discontinuity between the lower and the upper Earth's mantle is formulated in Section 4.1, leading to the barotropic state equation with the discontinuity at the specific phase-transition pressure which is at the depth 660 km. The space finite-element discretization and implementation for the resulting system of nonlinear algebraic equations at each time level are briefly outlined in Section 4.2. In Section 4.3, a 2D simulation of a phase transition within ascending plumes or descending slabs or stagnation (accompanied with a dehydration) of descending slabs will illustrate the above model as far as the applicability in geophysics concerns even in its isothermal variant as presented here. This represents a novelty, together with the generally applied numerically stable time discretization as devised and analysed in Section 3.

Let us summarize the main notation used in this paper in the following Table 1.

quantity	unit	explanation	quantity	unit	explanation
ϱ	$\mathrm{kg\,m^{-3}}$	mass density	φ_{R}	Pa	referential stored energy
$\boldsymbol{v}$	$\mathrm{m\,s^{-1}}$	velocity	$\varphi=\varphi_{\mathsf{R}}/J$	Pa	actual stored energy
p	Pa	total pressure	μ	Pa	chemical potential
π	Pa	partial pressure	$\kappa=\kappa(\chi,J)$	Pa	volume part φ (actual)
J	1	Jacobian	$\kappa_{\mathsf{R}}=\kappa_{\mathsf{R}}(\chi,J)$	Pa	volume part φ_{R} (referential)
c	1	diffusant (water) content	$\mathbb{D}=\mathbb{D}(J,\chi,c,\boldsymbol{\varepsilon}(\boldsymbol{v}))$	Pa s	viscosity tensor
B	Pa	Biot modulus	$f=f(\chi,c)$	$\mathrm{s^{-1}}$	water source
b	1	Biot coefficient	$m=m(J,\chi,c)$	$\mathrm{kg^{-1}m^2s}$	mobility of diffusant
χ	1	composition field	R	$\mathrm{kg\,m^{-3}}$	specific fluid density
$\boldsymbol{D}$	Pa	viscous stress	$\boldsymbol{\varepsilon}(\boldsymbol{v})=\frac{1}{2}\nabla\boldsymbol{v}^\top+\frac{1}{2}\nabla\boldsymbol{v}$	$\mathrm{s^{-1}}$	strain rate
$(\cdot)^{\cdot}$	$\mathrm{s^{-1}}$	convective time derivative	$V(\boldsymbol{x})=-\boldsymbol{g}\cdot\boldsymbol{x}$	$\mathrm{m^2\,s^{-2}}$	gravitational potential

Table 1: Summary of the basic notation with physical units.

2 The poro-visco-elastodynamic system

For the elastic response, we use concept of hyperelastic materials, where the Cauchy stress results from a stored-energy potential. Since we have in mind specific geophysical applications on long time scales, we consider here the elasticity only in the volumetric part without any elastic shear response except Remark 2.3. The conservative part of the Cauchy stress is thus of the pressure-type only and actually our model reduces to that of a viscoelastic fluid. We consider the diffusant to have a mass density that contributes to the energy. Therefore, the mass of the diffusant influences both the force under the prescribed gravitation field and also the diffusive flux via a phenomenological Rayleigh number compositional "influence" coefficient R, and it also contributes to the pressure so that the expected energetics is maintained. However, we make the simplifying assumption that the diffusant mass does not contribute to the kinetic energy.

The overall system for $(\varrho, \boldsymbol{v}, J, \chi, c)$ formulated in the referential stored energy $\varphi_{\mathsf{R}} = \varphi_{\mathsf{R}}(J, \chi, c)$ then consists of the mass continuity equation, the momentum equation, the kinematic equation for the Jacobian J, the transport of the composition field χ, and the diffusion/advection equation for the content c considered as an extensive variable. Specifically, this system reads as

$$\dot{\varrho} = -(\operatorname{div} \boldsymbol{v})\, \varrho\,, \tag{1a}$$

$$\varrho\dot{\boldsymbol{v}} - \operatorname{div} \boldsymbol{D} = \big(\varrho{+}Rc\big)\boldsymbol{g} - \nabla p \text{ where } \boldsymbol{D} = \mathbb{D}(J, \chi, c, \boldsymbol{\varepsilon}(\boldsymbol{v}))\boldsymbol{\varepsilon}(\boldsymbol{v}),\ \boldsymbol{g} = -\nabla V, \text{ and}$$
$$\text{where } p = \pi + c\mu \text{ with } \pi = -[\varphi_{\mathsf{R}}]'_J(J, \chi, c) - RcV\,, \tag{1b}$$

$$\dot{J} = (\operatorname{div} \boldsymbol{v})\, J\,, \tag{1c}$$

$$\dot{\chi} = 0\,, \tag{1d}$$

$$\dot{c} = \operatorname{div}\big(m(J, \chi, c)\nabla\mu\big) - (\operatorname{div} \boldsymbol{v})\, c + f(\chi, c) \quad \text{with } \mu = [\varphi_{\mathsf{R}}]'_c(J, \chi, c)/J + RV\,, \tag{1e}$$

where V denotes the (time-independent) gravitational potential (rescaled by involving the gravitational constant), *i.e.*, the gravitational acceleration is $\boldsymbol{g} = -\nabla V$. Note that the term stored energy for φ (actual) or φ_{R} (referential) is used synonymously with the term internal energy in our isothermal case.

It should be noted that, in view of (1a) and (1c), we have the relation $\varrho/J = \varrho_0/J_0$ where ϱ_0 and J_0 are initial conditions for the mentioned equations. When we would consider $J_0 = 1$ and ϱ_0 the referential mass density, one of these equations could be omitted when defining $\varrho = \varrho_0/J$ or $J = \varrho_0/\varrho$. Yet, sometimes the heterogeneous mass density or a non-constant J_0 is desirable, which is why we considered both these equations in the system (1). The other reason is for the time discretization of the full dynamic system where both equation (1a) and (1c) are discretized separately and the relation $\varrho/J = \varrho_0/J_0$ is satisfied only approximately in the discrete scheme, cf. Section 3.

The energetics of the system (1) can be seen by considering the system (26) on a fixed (Lipschitz) bounded domain $\Omega \subset \mathbb{R}^d$ with $d = 2$ or 3, and by testing of (1b) by $\boldsymbol{v}$ and of (1e) by μ when completing these equations by some boundary conditions, specifically

$$\boldsymbol{v}\cdot\boldsymbol{n} = 0\,, \quad \big((\boldsymbol{D}{-}p\mathbb{I})\boldsymbol{n}\big)_{\mathsf{T}} = \boldsymbol{0}\,, \quad \text{and } \nabla\mu\cdot\boldsymbol{n} = 0 \quad \text{on } \Gamma\,, \tag{2}$$

where $\boldsymbol{n}$ denotes the outward unit normal to Γ and where $(\cdot)_{\mathsf{T}}$ denotes the tangential component to the boundary Γ. This gives

$$\frac{\mathrm{d}}{\mathrm{d}t}\int_\Omega \frac{\varrho}{2}|\boldsymbol{v}|^2\,\mathrm{d}\boldsymbol{x} + \int_\Omega (\boldsymbol{D}{-}\pi\mathbb{I}) : \boldsymbol{\varepsilon}(\boldsymbol{v})\,\mathrm{d}\boldsymbol{x} = \int_\Omega c\mu \operatorname{div}\boldsymbol{v} - \big(\varrho{+}Rc\big)\nabla V\cdot\boldsymbol{v}\,\mathrm{d}\boldsymbol{x} \quad \text{and} \tag{3a}$$

$$\int_\Omega \frac{[\varphi_{\mathsf{R}}]'_c(J, \chi, c)}{J}\dot{c} + m(J, \chi, c)|\nabla\mu|^2\,\mathrm{d}\boldsymbol{x} = \int_\Omega f(\chi, c)\mu - c\,(\operatorname{div}\boldsymbol{v})\,\mu + R\dot{c}V\,\mathrm{d}\boldsymbol{x} \tag{3b}$$

In particular, reminding $\varphi_{\mathsf{R}}(J,\chi,c)=J\varphi(J,\chi,c)$, we use the calculus

$$\begin{aligned}
\int_\Omega \nabla\pi\cdot\boldsymbol{v}+\mu\dot c\,\mathrm{d}\boldsymbol{x} &= \int_\Omega \Big(\big[J\,\varphi(J,\chi,c)\big]'_J + RcV\Big)\mathrm{div}\,\boldsymbol{v}+\mu\dot c\,\mathrm{d}\boldsymbol{x}\\
&= \int_\Omega J\varphi'_J(J,\chi,c)\,\mathrm{div}\,\boldsymbol{v}+\big(\varphi(J,\chi,c)+RcV\big)\mathrm{div}\,\boldsymbol{v}+\mu\dot c\,\mathrm{d}\boldsymbol{x}\\
&\overset{(1c)}{=} \int_\Omega \varphi'_J(J,\chi,c)\dot J+\big(\varphi(J,\chi,c)+RcV\big)\mathrm{div}\,\boldsymbol{v}+\underbrace{\varphi'_\chi(J,\chi,c)\cdot\dot\chi}_{=\,0\text{ due to (1d)}}+\big(\varphi'_c(J,\chi,c)+RV\big)\dot c\,\mathrm{d}\boldsymbol{x}\\
&= \int_\Omega \dot{\overline{\varphi(J,\chi,c)+RcV}}+\big(\varphi(J,\chi,c)+RcV\big)\,\mathrm{div}\,\boldsymbol{v}\,\mathrm{d}\boldsymbol{x}\\
&= \frac{\mathrm{d}}{\mathrm{d}t}\int_\Omega \varphi(J,\chi,c)+RcV\,\mathrm{d}\boldsymbol{x}+\int_\Omega \boldsymbol{v}\cdot\nabla\big(\varphi(J,\chi,c)+RcV\big)+\big(\varphi(J,\chi,c)+RcV\big)\,\mathrm{div}\,\boldsymbol{v}\,\mathrm{d}\boldsymbol{x}\\
&= \frac{\mathrm{d}}{\mathrm{d}t}\int_\Omega \varphi(J,\chi,c)+RcV\,\mathrm{d}\boldsymbol{x}+\int_\Omega \mathrm{div}\big(\varphi(J,\chi,c)\,\boldsymbol{v}+RcV\boldsymbol{v}\big)\,\mathrm{d}\boldsymbol{x}\\
&= \frac{\mathrm{d}}{\mathrm{d}t}\int_\Omega \varphi(J,\chi,c)+RcV\,\mathrm{d}\boldsymbol{x}+\int_\Gamma \big(\varphi(J,\chi,c)+RcV\big)\ \underbrace{\boldsymbol{v}\cdot\boldsymbol{n}}_{=0}\ \mathrm{d}S\,.
\end{aligned}\tag{4}$$

Moreover, exploiting the mass continuity equation (1a) and the (time-independent) gravitational potential V of the gravitational acceleration $\boldsymbol{g}$, we still use

$$\int_\Omega \varrho\boldsymbol{v}\cdot\boldsymbol{g}\,\mathrm{d}\boldsymbol{x}=-\int_\Omega \varrho\boldsymbol{v}\cdot\nabla V\,\mathrm{d}\boldsymbol{x}=\int_\Omega \mathrm{div}(\varrho\boldsymbol{v})V\,\mathrm{d}\boldsymbol{x}-\int_\Gamma \varrho V\ \underbrace{\boldsymbol{v}\cdot\boldsymbol{n}}_{=0}\ \mathrm{d}S=-\frac{\mathrm{d}}{\mathrm{d}t}\int_\Omega \varrho V\,\mathrm{d}\boldsymbol{x}\,.\tag{5}$$

This gives the overall *energy-dissipation balance* as

$$\begin{aligned}
\frac{\mathrm{d}}{\mathrm{d}t}\int_\Omega \frac{\varrho}{2}|\boldsymbol{v}|^2+\varphi(J,\chi,c)+(\varrho+Rc)V\,\mathrm{d}\boldsymbol{x}+\int_\Omega m(J,\chi,c)|\nabla\mu|^2+\mathbb{D}(J,\chi,c,\boldsymbol{\varepsilon}(\boldsymbol{v}))\boldsymbol{\varepsilon}(\boldsymbol{v}):\boldsymbol{\varepsilon}(\boldsymbol{v})\,\mathrm{d}\boldsymbol{x}\\
=\int_\Omega f(\chi,c)\mu\,\mathrm{d}\boldsymbol{x}\,.
\end{aligned}\tag{6}$$

The "compensating" pressure $c\mu$ in (1b) resulting from the evolution of the extensive internal variable c and which led to the cancellation in (3) was revealed by a so-called GENERIC framework in [23]. Also, notably, the "Helmholtz-type" referential stored energy φ_{R} could be considered extended to a referential "Gibbs-type" stored energy

$$\varphi_{\mathsf{G}}(J,\chi,c):=\varphi_{\mathsf{R}}(J,\chi,c)+RJcV\tag{7}$$

and then we could write simply $\pi=-[\varphi_{\mathsf{G}}]'_J(J,\chi,c)$ in (1b) and $\mu=[\varphi_{\mathsf{G}}]'_c(J,\chi,c)/J$ in (1e).

Remark 2.1 (*Modelling of mass diffusant*)**.** A certain dichotomy of the mass diffusant approximation is that is not involved in the inertia on its left-hand side but its mass is involved in the right-hand-side force, actually through the dimensionless compositional coefficient that characterizes the behaviour of fluids in natural convection, particularly when density differences, and in the pressure in (1b) and also in the diffusive flux in (1e). Related to it, we should also note that (7) depends on the values of the gravitational potential V so that V should be reasonably fixed.

Remark 2.2 (*Quasistatic variant of (12)*)**.** In geophysical modelling focused to mantle dynamics in long time scales (as descenting slabs, ascending plumes, volcanic chambers, etc.) does not involve inertial force, *i.e.*, quasistatic (also called quasidynamic) models. Neglecting the inertial force $\varrho\dot{\boldsymbol{v}}$ allows easily for omitting the continuity equation for ϱ when using the equation for J. This, together with a cancellation of the RV terms (1b)

and (1e) in the total pressure p, simplifies (12) to the system for $(\boldsymbol{v}, J, \chi, c)$:

$$\operatorname{div}\boldsymbol{D} = \nabla p + \Big(\frac{\varrho_0}{J} + Rc\Big)\nabla V \quad \text{with } p = -J\varphi'_J(J,\chi,c) + c\varphi'_c(J,\chi,c) - \varphi(J,\chi,c) + RcV \text{ and}$$
$$\text{with } \boldsymbol{D} = \mathbb{D}(J,\chi,c,\boldsymbol{\varepsilon}(\boldsymbol{v}))\boldsymbol{\varepsilon}(\boldsymbol{v}) - \operatorname{div}\big(\nu|\nabla^2\boldsymbol{v}|^{q-2}\nabla^2\boldsymbol{v}\big)\,, \tag{8a}$$
$$\frac{\partial J}{\partial t} = (\operatorname{div}\boldsymbol{v})\,J - \boldsymbol{v}\cdot\nabla J\,, \tag{8b}$$
$$\frac{\partial \chi}{\partial t} = -\boldsymbol{v}\cdot\nabla\chi\,, \tag{8c}$$
$$\frac{\partial c}{\partial t} = \operatorname{div}\big(m(J,\chi,c)\nabla\mu - c\,\boldsymbol{v}\big) + f(\chi,c) \quad \text{with } \mu = \varphi'_c(J,\chi,c) + RV\,. \tag{8d}$$

The a-priori estimates derived from the energy-dissipation balance without the kinetic energy then rely on a sufficiently fast blow-up of φ for $J \to 0+$. Moreover, the boundary conditions (13) have to be modified by prescribing the full Dirichlet condition at least on a part of the boundary to control a rigid-body motion.

Remark 2.3 (*Poro-elastic solids)***.** A general inelastic solids at large strains relies on the multiplicative decomposition of the deformation gradient $\boldsymbol{F}$ to the elastic and the (isochoric) inelastic distortions $\boldsymbol{F}_{\rm e}$ and $\boldsymbol{F}_{\rm p}$, cf. *e.g.* [6, 32]. The elastic response can then be involved not only in the volumetric part but also in the isochoric part considering the Maxwell (or Jeffreys) rheology. Then, we would come to evolution of the full elastic distortion $\boldsymbol{F}_{\rm e}$. Relying on the neo-Hookean ansatz in the reference configuration with $G_{\rm E}$ the shear elastic modulus, we set

$$\varphi_{\rm R}(\boldsymbol{F}_{\rm e},J,c) = \kappa_{\rm R}(J) + G_{\rm E}|\boldsymbol{F}_{\rm v}|^2 + \frac{B}{2}\big(c+b(J-J_{\rm PT})\big)^2 + \epsilon Jc\Big(\ln\frac{c}{c_0}-1\Big) \text{ with } \boldsymbol{F}_{\rm v} = \frac{\boldsymbol{F}_{\rm e}}{J^{1/3}}; \tag{9}$$

here we have in mind 3D situation. This $G_{\rm E}$-term gives the contribution to the Cauchy stress

$$G_{\rm E}\left[\frac{|\boldsymbol{F}_{\rm e}|^2}{(\det\boldsymbol{F}_{\rm e})^{2/3}}\right]'\frac{\boldsymbol{F}_{\rm e}^\top}{\det\boldsymbol{F}_{\rm e}} = 2G_{\rm E}\frac{\boldsymbol{F}_{\rm e}\boldsymbol{F}_{\rm e}^\top}{(\det\boldsymbol{F}_{\rm e})^{5/3}} - \frac{2}{3}G_{\rm E}\frac{|\boldsymbol{F}_{\rm e}|^2}{(\det\boldsymbol{F}_{\rm e})^{2/3}}\mathbb{I}\,.$$

The overall Cauchy stress $\boldsymbol{T} = \boldsymbol{T}(\boldsymbol{F}_{\rm e},c) = [\varphi_{\rm R}(\boldsymbol{F}_{\rm e},\det\boldsymbol{F}_{\rm e},c)]'_{\boldsymbol{F}_{\rm e}}\boldsymbol{F}_{\rm e}^\top/\det\boldsymbol{F}_{\rm e}$ written in terms of the isochoric part $\boldsymbol{F}_{\rm v}$ of $\boldsymbol{F}_{\rm e}$ is

$$\boldsymbol{T} = 2G_{\rm E}\frac{\boldsymbol{F}_{\rm v}\boldsymbol{F}_{\rm v}^\top}{J} - \Big(\frac{2}{3}G_{\rm E}|\boldsymbol{F}_{\rm v}|^2 + p\Big)\mathbb{I} \quad \text{with } p = -[\varphi_{\rm R}]'_J(J,c)\,. \tag{10}$$

Notably, the actual stored energy corresponding to (9) is of the polyconvex type in terms of $(\boldsymbol{F}_{\rm v},J,c)$, which facilitates stability of the implicit time discretization. Considering the linear Maxwellian viscosity with the viscosity modulus $G_{\rm M} > 0$ and ignoring (for simplicity) the composition field χ, this results to the system for $(\varrho,\boldsymbol{v},\boldsymbol{F}_{\rm v},c)$:

$$\dot\varrho = -(\operatorname{div}\boldsymbol{v})\,\varrho\,, \tag{11a}$$
$$\varrho\dot{\boldsymbol{v}} - \operatorname{div}\Big(\mathbb{D}\boldsymbol{\varepsilon}(\boldsymbol{v}) + 2G_{\rm E}\frac{\boldsymbol{F}_{\rm v}\boldsymbol{F}_{\rm v}^\top}{J}\Big) + \nabla\Big(\frac{2}{3}G_{\rm E}|\boldsymbol{F}_{\rm v}|^2 - [\varphi_{\rm R}]'_J(J,c) + \frac{c}{J}[\varphi_{\rm R}]'_c(J,c)\Big) = -\big(\varrho+Rc\big)\nabla V, \tag{11b}$$
$$\dot J = (\operatorname{div}\boldsymbol{v})\,J\,, \tag{11c}$$
$$\dot{\boldsymbol{F}}_{\rm v} = (\nabla\boldsymbol{v})\boldsymbol{F}_{\rm v} - \frac{1}{3}(\operatorname{div}\boldsymbol{v})\boldsymbol{F}_{\rm v} - 2\frac{G_{\rm E}}{G_{\rm M}}\boldsymbol{F}_{\rm v}\frac{\boldsymbol{F}_{\rm v}\boldsymbol{F}_{\rm v}^\top}{J}, \tag{11d}$$
$$\dot c = \operatorname{div}\big(m(J,c)\nabla\mu\big) - (\operatorname{div}\boldsymbol{v})\,c + f(c) \quad \text{with } \mu = [\varphi_{\rm R}]'_c(J,c)/J + RV\,. \tag{11e}$$

The equation (11d) for the isochoric part of the elastic distortion $\boldsymbol{F}_{\rm v}$ can be derived by using the multiplicative decomposition $\boldsymbol{F} = \boldsymbol{F}_{\rm p}\boldsymbol{F}_{\rm e}$ with the chain rule $\dot{\boldsymbol{F}} = (\nabla\boldsymbol{v})\boldsymbol{F}$ and the flow rule for the inelastic distortion $G_{\rm M}\dot{\boldsymbol{F}}_{\rm p} = \operatorname{dev}\boldsymbol{M}$ with the Mandel stress $\boldsymbol{M} = \boldsymbol{F}_{\rm e}^\top\varphi'_{\boldsymbol{F}_{\rm e}}(\boldsymbol{F}_{\rm e},\det\boldsymbol{F}_{\rm e},c)$.

3 The time discretization and analysis in a multipolar variant

In the following we address the mathematical analysis of (a regularized version of) model (1) in space dimension $d \in \{2,3\}$. To this aim, we rewrite the system in terms of the linear momentum $\boldsymbol{p} = \varrho \boldsymbol{v}$. Moreover, we formulate the system in terms of the actual stored energy $\varphi = \varphi_{\mathsf{R}}/J$. Note that, compared to (1), due to this change of frame, different terms arise in the pressure p and in the chemical potential μ, cf. (12b) and (12e) below. For the analysis, we will introduce a (for simplicity equidistant) time discretization, exploiting the fully implicit backward Euler formula (i.e. Rothe's method) combined with suitable regularizing terms. This also suggests an implementable numerical strategy. The numerical stability with respect to the time step $\tau > 0$ will be guaranteed, but the convergence for $\tau \to 0$ and thus existence of some weak solutions will be proved only when modifying the Stokes-type viscosity by some higher-order gradient term. This is the concept of so-called multipolar (also known as nonsimple) media, here considered as nonlinear 2nd-grade, which leads to a so-called hyperstress $\mathfrak{H}$, cf. (12b). The physical theory of multipolar fluids appeared in [26] following the general ideas of Green and Rivlin [15]. See also [14, 25].

By this way, we arrive to the system for $(\varrho, \boldsymbol{v}, J, \chi, c)$ and thus also for $\boldsymbol{p}$:

$$\frac{\partial \varrho}{\partial t} = -\operatorname{div} \boldsymbol{p} \quad \text{with } \boldsymbol{p} = \varrho \boldsymbol{v}\,, \tag{12a}$$

$$\begin{aligned}\frac{\partial \boldsymbol{p}}{\partial t} &= \operatorname{div}\big(\boldsymbol{D} - \boldsymbol{p}\otimes\boldsymbol{v}\big) - \nabla p - \big(\varrho + Rc\big)\nabla V \\ &\qquad \text{with } p = c\varphi_c'(J,\chi,c) - J\varphi_J'(J,\chi,c) - \varphi(J,\chi,c) \text{ and} \\ &\qquad \text{with } \boldsymbol{D} = \mathbb{D}(J,\chi,c,\boldsymbol{\varepsilon}(\boldsymbol{v}))\boldsymbol{\varepsilon}(\boldsymbol{v}) - \operatorname{div}\mathfrak{H} \text{ where } \mathfrak{H} = \nu|\nabla^2\boldsymbol{v}|^{q-2}\nabla^2\boldsymbol{v}\,,\end{aligned} \tag{12b}$$

$$\frac{\partial J}{\partial t} = (\operatorname{div}\boldsymbol{v})\, J - \boldsymbol{v}\cdot\nabla J\,, \tag{12c}$$

$$\frac{\partial \chi}{\partial t} = -\boldsymbol{v}\cdot\nabla\chi\,, \tag{12d}$$

$$\frac{\partial c}{\partial t} = \operatorname{div}\big(m(J,\chi,c)\nabla\mu - c\boldsymbol{v}\big) + f(\chi,c) \quad \text{with } \mu = \varphi_c'(J,\chi,c) + RV\,. \tag{12e}$$

Due to the hyperstress $\mathfrak{H}$ in (12b), the boundary conditions (2) must be adapted accordingly as

$$\boldsymbol{v}\cdot\boldsymbol{n} = 0\,, \quad \big((\boldsymbol{D} - p\mathbb{I})\boldsymbol{n} - \operatorname{div}_{\mathrm{s}}(\mathfrak{H}\boldsymbol{n})\big)_{\mathsf{T}} = \boldsymbol{0}\,, \quad \nabla^2\boldsymbol{v} : (\boldsymbol{n}\otimes\boldsymbol{n}) = \boldsymbol{0}\,, \text{ and } \nabla\mu\cdot\boldsymbol{n} = 0 \text{ on } \Gamma\,, \tag{13}$$

where the $(d-1)$-dimensional surface divergence is defined as

$$\operatorname{div}_{\mathrm{s}} = \operatorname{tr}(\nabla_{\mathrm{s}}) \quad \text{with } \nabla_{\mathrm{s}} v = \nabla v - \frac{\partial v}{\partial \boldsymbol{n}}\boldsymbol{n}\,. \tag{14}$$

Here $\operatorname{tr}(\cdot)$ is the trace of a $(d-1)\times(d-1)$-matrix and $\nabla_{\mathrm{s}} v$ is the surface gradient of v. The overall energy-dissipation balance (6) now modifies as

$$\begin{aligned}\frac{\mathrm{d}}{\mathrm{d}t}\int_\Omega \frac{|\boldsymbol{p}|^2}{2\varrho} + \varphi(J,\chi,c) + \big(\varrho + Rc\big)V \,\mathrm{d}\boldsymbol{x} + \int_\Omega m(J,\chi,c)|\nabla\mu|^2 + \mathbb{D}(J,\chi,c,\boldsymbol{\varepsilon}(\boldsymbol{v}))|\boldsymbol{\varepsilon}(\boldsymbol{v})|^2 + \nu|\nabla^2\boldsymbol{v}|^q \,\mathrm{d}\boldsymbol{x} \\ = \int_\Omega f(\chi,c)\mu \,\mathrm{d}\boldsymbol{x}\,.\end{aligned} \tag{15}$$

Moreover, we consider the initial conditions

$$\varrho\big|_{t=0} = \varrho_0\,, \quad \boldsymbol{p}\big|_{t=0} = \boldsymbol{p}_0\,, \quad J\big|_{t=0} = J_0\,, \quad \chi\big|_{t=0} = \chi_0\,, \text{ and } c\big|_{t=0} = c_0\,. \tag{16}$$

Note that this actually determines also the initial velocity $\boldsymbol{v}\big|_{t=0} = \boldsymbol{p}_0/\varrho_0$.

Definition 3.1 (Weak solutions to (12)). *The six-tuple* $(\varrho, \boldsymbol{v}, J, \chi, c, \mu)$ *with*

$$\varrho \in L^\infty(I; W^{1,r}(\Omega)) \cap C(I\times\bar\Omega)\,, \tag{17a}$$
$$\boldsymbol{v} \in L^\infty(I; L^2(\Omega;\mathbb{R}^d)) \cap L^q(I; W^{2,q}(\Omega;\mathbb{R}^d))\,, \tag{17b}$$
$$J,\ \chi \in L^\infty(I; W^{1,r}(\Omega)) \cap C(I\times\bar\Omega)\,, \tag{17c}$$
$$c \in L^\infty(I; L^2(\Omega)) \cap L^2(I; H^2(\Omega)) \quad \textit{and} \quad \mu = \varphi_c'(J,c) + RV \ \textit{a.e. on}\ I\times\Omega\,, \tag{17d}$$

such that also

$$m(J,\chi,c)\nabla\mu \in L^1(I\times\Omega;\mathbb{R}^d)\,,\quad c\mu \in L^1(I\times\Omega) \quad \textit{as well as} \quad f(\chi,c)\mu \in L^1(I\times\Omega)$$

will be called a weak solution to the Eulerian poro-visco-elastodynamic system (12) with the initial and boundary conditions (13) and (16) if

- *the transport equations (12a), (12c), (12d) hold a.e. on* $I\times\Omega$ *with the initial conditions* $\varrho\big|_{t=0} = \varrho_0$, $J\big|_{t=0} = J_0$, *and* $\chi\big|_{t=0} = \chi_0$;
- *there holds* $\boldsymbol{v}\cdot\boldsymbol{n} = 0$ *a.e. in* $I\times\Gamma$ *as well as* $J > 0$ *a.e. in* $I\times\Omega$, *and the momentum balance* (12b) *is satisfied in the weak form*

$$\int_0^T\!\!\int_\Omega \Big(\mathbb{D}(J,\chi,c,\boldsymbol{\varepsilon}(\boldsymbol{v}))\boldsymbol{\varepsilon}(\boldsymbol{v}) - \varrho\boldsymbol{v}\otimes\boldsymbol{v}\Big) : \boldsymbol{\varepsilon}(\widetilde{\boldsymbol{v}}) - \varrho\boldsymbol{v}\cdot\frac{\partial\widetilde{\boldsymbol{v}}}{\partial t} + \nu|\nabla^2\boldsymbol{v}|^{q-2}\nabla^2\boldsymbol{v}\,\vdots\,\nabla^2\widetilde{\boldsymbol{v}} - p\,\mathrm{div}\,\widetilde{\boldsymbol{v}}\,\mathrm{d}\boldsymbol{x}\mathrm{d}t$$
$$= \int_\Omega \varrho_0\boldsymbol{v}_0\cdot\widetilde{\boldsymbol{v}}(0)\,\mathrm{d}\boldsymbol{x} - \int_0^T\!\!\int_\Omega \big(\varrho + Rc\big)\nabla V\cdot\widetilde{\boldsymbol{v}}\,\mathrm{d}\boldsymbol{x}\mathrm{d}t \tag{18a}$$

  with $p = c\varphi_c'(J,\chi,c) - J\varphi_J'(J,\chi,c) - \varphi(J,\chi,c)$, *for any smooth function* $\widetilde{\boldsymbol{v}}$ *with* $\widetilde{\boldsymbol{v}}\cdot\boldsymbol{n} = 0$ *and* $\widetilde{\boldsymbol{v}}(T) = 0$;

- *the following weak formulation of the diffusion equation* (12e) *holds true*

$$\int_0^T\!\!\int_\Omega m(J,\chi,c)\nabla\mu\cdot\nabla\tilde c - c\cdot\frac{\partial\tilde c}{\partial t} + c\boldsymbol{v}\cdot\nabla\tilde c - f(\chi,c)\,\tilde c\,\mathrm{d}\boldsymbol{x}\mathrm{d}t = \int_\Omega c_0\cdot\tilde c(0)\,\mathrm{d}\boldsymbol{x} \tag{18b}$$

  for all smooth functions $\tilde c$ *with* $\tilde c(T) = 0$.

For the analysis we will intermediately augment system (12) by a further regularization in terms of an r-Laplacian of the mass density for some $r > d$, which will be scaled by another parameter $\delta > 0$. Thus, taking into account these afore-mentioned regularizing terms scaled by the parameters $\varepsilon > 0$ and $\delta > 0$ in (12), leads to the following regularized system (19), whose solutions we will denote by the tuple $(\varrho_{\varepsilon\delta}, \boldsymbol{p}_{\varepsilon\delta}, J_{\varepsilon\delta}, \chi_{\varepsilon\delta}, c_{\varepsilon\delta})$ and also $(\boldsymbol{v}_{\varepsilon\delta}, \mu_{\varepsilon\delta})$:

$$\frac{\partial\varrho_{\varepsilon\delta}}{\partial t} = \mathrm{div}\big(\delta|\nabla\varrho_{\varepsilon\delta}|^{r-2}\nabla\varrho_{\varepsilon\delta} - \mathcal{I}(\varrho_{\varepsilon\delta})\boldsymbol{p}_{\varepsilon\delta}\big) \ \text{ with } \ \boldsymbol{p}_{\varepsilon\delta} = \varrho_{\varepsilon\delta}\boldsymbol{v}_{\varepsilon\delta}\,, \tag{19a}$$

$$\frac{\partial\boldsymbol{p}_{\varepsilon\delta}}{\partial t} = \mathrm{div}\Big(\boldsymbol{D}_{\varepsilon\delta} - \mathcal{I}(\varrho_{\varepsilon\delta})\boldsymbol{p}_{\varepsilon\delta}\otimes\boldsymbol{v}_{\varepsilon\delta}\Big) - \nabla p_{\varepsilon\delta} - \big(\varrho_{\varepsilon\delta} + Rc_{\varepsilon\delta}\big)\nabla V$$
$$- \varepsilon|\boldsymbol{v}_{\varepsilon\delta}|^{q-2}\boldsymbol{v}_{\varepsilon\delta} - \delta|\nabla\varrho_{\varepsilon\delta}|^{r-2}(\nabla\boldsymbol{v}_{\varepsilon\delta})\nabla\varrho_{\varepsilon\delta}\,,$$
$$\text{where } \ \boldsymbol{D}_{\varepsilon\delta} = \mathbb{D}(J_{\varepsilon\delta},\chi_{\varepsilon\delta},c_{\varepsilon\delta},\boldsymbol{\varepsilon}(\boldsymbol{v}_{\varepsilon\delta}))\boldsymbol{\varepsilon}(\boldsymbol{v}_{\varepsilon\delta}) - \mathrm{div}\big(\nu\big|\nabla^2\boldsymbol{v}_{\varepsilon\delta}\big|^{q-2}\nabla^2\boldsymbol{v}_{\varepsilon\delta}\big)\,,\ \text{and}$$
$$\text{where } \ p_{\varepsilon\delta} = c_{\varepsilon\delta}\varphi_c'(J_{\varepsilon\delta},\chi_{\varepsilon\delta},c_{\varepsilon\delta}) - J_{\varepsilon\delta}\varphi_J'(J_{\varepsilon\delta},\chi_{\varepsilon\delta},c_{\varepsilon\delta}) - \varphi(J_{\varepsilon\delta},\chi_{\varepsilon\delta},c_{\varepsilon\delta}), \tag{19b}$$

$$\frac{\partial J_{\varepsilon\delta}}{\partial t} = (\mathrm{div}\,\boldsymbol{v}_{\varepsilon\delta})J_{\varepsilon\delta} - \boldsymbol{v}_{\varepsilon\delta}\cdot\nabla J_{\varepsilon\delta}\,, \tag{19c}$$

$$\frac{\partial\chi_{\varepsilon\delta}}{\partial t} = -\boldsymbol{v}_{\varepsilon\delta}\cdot\nabla\chi_{\varepsilon\delta}\,, \tag{19d}$$

$$\frac{\partial c_{\varepsilon\delta}}{\partial t} = \mathrm{div}\,\big(m(J_{\varepsilon\delta},\chi_{\varepsilon\delta},c_{\varepsilon\delta})\nabla\mu_{\varepsilon\delta} - c_{\varepsilon\delta}\boldsymbol{v}_{\varepsilon\delta}\big) + f(\chi_{\varepsilon\delta},c_{\varepsilon\delta}) \ \text{ with } \ \mu_{\varepsilon\delta} = \varphi_c'(J_{\varepsilon\delta},\chi_{\varepsilon\delta},c_{\varepsilon\delta}) + RV\,. \tag{19e}$$

Here we have used a cut-off function $\mathcal{I}$ in (19a) and (19b), which is defined as follows

$$\mathcal{I}(\varrho) := \begin{cases} 1 & \text{for } 0 \le \varrho \le \rho_{\max}, \\ 0 & \text{for } \varrho < 0 \text{ or } \varrho \ge \rho_{\max}+1, \\ \in [0,1] & \text{for } \rho_{\max} < \varrho < \rho_{\max}+1 \end{cases} \tag{20}$$

with some $0 < \rho_{\max}$ to be chosen later. In fact, despite of the discontinuity of $\mathcal{I}$ at 0, the function $\varrho \mapsto \mathcal{I}(\varrho)\varrho$ is a Lipschitz continuous, non-negative function. We also refer to [24, 38], where the idea of a cut-off for the mass density has already been used in the context of compressible Navier-Stokes equations. We complete system (19) by the boundary condition (13) written for the (ε,δ)-solution and additionally by the condition

$$\nabla \varrho_{\varepsilon\delta} \cdot \boldsymbol{n} = 0 \quad \text{on } \Gamma\,. \tag{21}$$

Using an equidistant discretization $t_\tau^0 = 0 < t_\tau^1 < \ldots < t_\tau^{T/\tau} = T$ of the time interval $[0,T]$ in terms of the time-step size τ with $T/\tau \in \mathbb{N}$ we then devise the recursive regularized time-discrete scheme. To this aim, we use the fully implicit time discretization of (19). For every $k \in \{1,\ldots,T/\tau\}$ the tuple $(\varrho^k_{\varepsilon\delta\tau}, \boldsymbol{p}^k_{\varepsilon\delta\tau}, J^k_{\varepsilon\delta\tau}, \chi^k_{\varepsilon\delta\tau}, c^k_{\varepsilon\delta\tau})$, and thus also $\boldsymbol{v}^k_{\varepsilon\delta\tau}$ and $\mu^k_{\varepsilon\delta\tau}$, is determined by the following time-discrete system

$$\frac{\varrho^k_{\varepsilon\delta\tau}-\varrho^{k-1}_{\varepsilon\delta\tau}}{\tau} = \operatorname{div}\big(\delta|\nabla\varrho^k_{\varepsilon\delta\tau}|^{r-2}\nabla\varrho^k_{\varepsilon\delta\tau} - \mathcal{I}(\varrho^k_{\varepsilon\delta\tau})\boldsymbol{p}^k_{\varepsilon\delta\tau}\big) \text{ with } \boldsymbol{p}^k_{\varepsilon\delta\tau} = \varrho^k_{\varepsilon\delta\tau}\boldsymbol{v}^k_{\varepsilon\delta\tau}\,, \tag{22a}$$

$$\begin{aligned}\frac{\boldsymbol{p}^k_{\varepsilon\delta\tau}-\boldsymbol{p}^{k-1}_{\varepsilon\delta\tau}}{\tau} &= \operatorname{div}\Big(\boldsymbol{D}^k_{\varepsilon\delta\tau} - \mathcal{I}(\varrho^k_{\varepsilon\delta\tau})\boldsymbol{p}^k_{\varepsilon\delta\tau}\otimes\boldsymbol{v}^k_{\varepsilon\delta\tau}\Big) - \nabla p^k_{\varepsilon\delta\tau} - \big(\varrho^k_{\varepsilon\delta\tau}+Rc^k_{\varepsilon\delta\tau}\big)\nabla V \\ &\qquad - \varepsilon|\boldsymbol{v}^k_{\varepsilon\delta\tau}|^{q-2}\boldsymbol{v}^k_{\varepsilon\delta\tau} - \delta|\nabla\varrho^k_{\varepsilon\delta\tau}|^{r-2}(\nabla\boldsymbol{v}^k_{\varepsilon\delta\tau})\nabla\varrho^k_{\varepsilon\delta\tau}\,,\end{aligned}$$

$$\text{where } \boldsymbol{D} = \mathbb{D}^k_{\varepsilon\delta\tau}\boldsymbol{\varepsilon}(\boldsymbol{v}^k_{\varepsilon\delta\tau}) - \operatorname{div}\big(\nu\big|\nabla^2\boldsymbol{v}^k_{\varepsilon\delta\tau}\big|^{q-2}\nabla^2\boldsymbol{v}^k_{\varepsilon\delta\tau}\big) \text{ with } \mathbb{D}^k_{\varepsilon\delta\tau} = \mathbb{D}(J^k_{\varepsilon\delta\tau}, \chi^k_{\varepsilon\delta\tau}, c^k_{\varepsilon\delta\tau}, \boldsymbol{\varepsilon}(\boldsymbol{v}^k_{\varepsilon\delta\tau}))$$

$$\text{and } p^k_{\varepsilon\delta\tau} = c^k_{\varepsilon\delta\tau}\varphi_c'(J^k_{\varepsilon\delta\tau}, \chi^k_{\varepsilon\delta\tau}, c^k_{\varepsilon\delta\tau}) - J^k_{\varepsilon\delta\tau}\varphi_J'(J^k_{\varepsilon\delta\tau}, \chi^k_{\varepsilon\delta\tau}, c^k_{\varepsilon\delta\tau}) - \varphi(J^k_{\varepsilon\delta\tau}, \chi^k_{\varepsilon\delta\tau}, c^k_{\varepsilon\delta\tau})\,, \tag{22b}$$

$$\frac{J^k_{\varepsilon\delta\tau}-J^{k-1}_{\varepsilon\delta\tau}}{\tau} = (\operatorname{div}\boldsymbol{v}^k_{\varepsilon\delta\tau})J^k_{\varepsilon\delta\tau} - \boldsymbol{v}^k_{\varepsilon\delta\tau}\cdot\nabla J^k_{\varepsilon\delta\tau}\,, \tag{22c}$$

$$\frac{\chi^k_{\varepsilon\delta\tau}-\chi^{k-1}_{\varepsilon\delta\tau}}{\tau} = -\boldsymbol{v}^k_{\varepsilon\delta\tau}\cdot\nabla\chi^k_{\varepsilon\delta\tau}\,, \tag{22d}$$

$$\begin{aligned}\frac{c^k_{\varepsilon\delta\tau}-c^{k-1}_{\varepsilon\delta\tau}}{\tau} &= \operatorname{div}\big(m^k_{\varepsilon\delta\tau}\nabla\mu^k_{\varepsilon\delta\tau} - c^k_{\varepsilon\delta\tau}\boldsymbol{v}^k_{\varepsilon\delta\tau}\big) + f(\chi^k_{\varepsilon\delta\tau}, c^k_{\varepsilon\delta\tau}) \text{ with } \mu^k_{\varepsilon\delta\tau} = \varphi_c'(J^k_{\varepsilon\delta\tau}, \chi^k_{\varepsilon\delta\tau}, c^k_{\varepsilon\delta\tau}) + RV \\ &\qquad \text{and } m^k_{\varepsilon\delta\tau} = m(J^k_{\varepsilon\delta\tau}, \chi^k_{\varepsilon\delta\tau}, c^k_{\varepsilon\delta\tau})\,,\end{aligned} \tag{22e}$$

completed by the boundary conditions (13) and (21) and by the following initial conditions

$$\varrho^0_{\varepsilon\delta\tau} = \varrho_0\,, \qquad \boldsymbol{p}^0_{\varepsilon\delta\tau} = \varrho_0\boldsymbol{v}_0\,, \qquad J^0_{\varepsilon\delta\tau} = J_0\,, \qquad \chi^0_{\varepsilon\delta\tau} = \chi_0\,, \quad \text{and} \quad c^0_{\varepsilon\delta\tau} = c_0\,. \tag{23}$$

Next, we summarize the assumptions on the data for some exponents $q > r > d$:

$$\varphi \in C^1(\mathbb{R}^+\times\mathbb{R}\times\mathbb{R}^+) \text{ convex, piecewise } C^2\,,\ \ m \in C(\mathbb{R}^+\times\mathbb{R}\times\mathbb{R}^+)\,, \tag{24a}$$

$$\exists\, s > \frac{rd}{r-d}\ \exists\,\eta>0\ \ \forall (J,\chi,c)\in\mathbb{R}^+\times\mathbb{R}\times\mathbb{R}^+\colon\ \ \varphi(J,\chi,c) \geq \frac{1}{\eta}J^{-s} + \eta J + \eta c^2 - \frac{1}{\eta}\,, \tag{24b}$$

$$\begin{aligned}\exists\,\eta\in(0,3)\ \ \forall 0<a<b<+\infty:\quad & \inf_{a\leq J\leq b,\ c\in(0,+\infty)} m(J,\chi,c)\,\varphi''_{cc}(J,\chi,c) > 0\,,\\ & \sup_{a\leq J\leq b,\ c\in(0,+\infty)} m(J,\chi,c)\,\varphi''_{cc}(J,\chi,c)/(1+c^{3-\eta}) < +\infty\,,\ \text{ and}\\ & \sup_{a\leq J\leq b,\ c\in(0,+\infty)} m(J,\chi,c)\,|\varphi''_{Jc}(J,\chi,c)|/(1+c) < +\infty\,,\end{aligned} \tag{24c}$$

$$\nu>0\,,\ \ \mathbb{D}\in C(\mathbb{R}\times\mathbb{R}\times\mathbb{R}\times\mathbb{R}^{d\times d};\mathbb{R}^{d\times d}) \text{ and } \exists\, 0<\eta_1\leq\eta_2<\infty\ \ \forall(J,\chi,c,\boldsymbol{\varepsilon},\tilde{\boldsymbol{\varepsilon}})\in\mathbb{R}^3\times\mathbb{R}^{d\times d}\times\mathbb{R}^{d\times d}:$$
$$\eta_1|\tilde{\boldsymbol{\varepsilon}}|^2 \leq \mathbb{D}(J,\chi,c,\boldsymbol{\varepsilon})\tilde{\boldsymbol{\varepsilon}}{:}\tilde{\boldsymbol{\varepsilon}} \leq \eta_2|\tilde{\boldsymbol{\varepsilon}}|^2\,, \tag{24d}$$

$$\exists\, 1\leq a<10/3\ \exists\,\eta>0\ \ \forall(J,\chi,c)\in\mathbb{R}^+\times\mathbb{R}\times\mathbb{R}^+:\ \ \ 0\leq m(J,\chi,c)\leq\frac{1}{\eta}(1+c^a)\,, \tag{24e}$$

$$f\in C(\mathbb{R}\times\mathbb{R}^+)\,,\ \ \exists\,\eta>0\ \ \forall(J,c)\in\mathbb{R}^+\times\mathbb{R}^+:\ \ \ \big|f(\chi,c)\,\varphi'_c(J,\chi,c)\big| \leq \frac{1}{\eta}\big(1+J+c^2\big)\,, \tag{24f}$$

$$\forall J,\chi\geq 0,\ c\leq 0:\quad m(J,\chi,c)=0\,,\quad m'_J(J,\chi,c)=m'_\chi(J,\chi,c)=0\,,\ \text{ and }\ f(\chi,c)\geq 0\,, \tag{24g}$$

$$\varrho_0, J_0, \chi_0 \in W^{1,r}(\Omega)\,,\ \ \min_{\bar\Omega}\varrho_0>0\,,\ \ \min_{\bar\Omega}J_0>0\,,\ \ \boldsymbol{v}_0\in L^2(\Omega;\mathbb{R}^d)\,, \tag{24h}$$

$$c_0\in L^2(\Omega),\ \ c_0>0 \text{ a.e. on } \Omega\,,\ \ \varphi(J_0,\chi_0,c_0)\in L^1(\Omega),\ \ V\in C^1(\bar\Omega)\,. \tag{24i}$$

We refer to Examples 3.3 and 3.4 below for a further discussion of the assumptions and examples of stored energy functions that are compatible with (24). Below we will use the notation with interpolants in time defined as follows: for the solutions $(\varrho^k_{\varepsilon\delta\tau}, \boldsymbol{p}^k_{\varepsilon\delta\tau}, J^k_{\varepsilon\delta\tau}, \chi^k_{\varepsilon\delta\tau}, c^k_{\varepsilon\delta\tau})_{k=0}^{T/\tau}$ of problem (22), resp. also for $(\boldsymbol{v}^k_{\varepsilon\delta\tau})_{k=0}^{T/\tau}$ and $(\mu^k_{\varepsilon\delta\tau})_{k=0}^{T/\tau}$, we define the piecewise constant and the piecewise affine interpolants respectively, as

$$\overline{\boldsymbol{v}}_{\varepsilon\delta\tau}(t) := \boldsymbol{v}^k_{\varepsilon\delta\tau} \quad\text{and}\quad \boldsymbol{v}_{\varepsilon\delta\tau}(t) := \Big(\frac{t}{\tau}-k+1\Big)\boldsymbol{v}^k_{\varepsilon\delta\tau} + \Big(k-\frac{t}{\tau}\Big)\boldsymbol{v}^{k-1}_{\varepsilon\delta\tau} \quad\text{for } (k-1)\tau<t\leq k\tau \tag{25}$$

for $k=0,1,\dots,T/\tau$; analogously, we define also $\underline{\varrho}_{\varepsilon\delta\tau}$, $\varrho_{\varepsilon\delta\tau}$, $\overline{\boldsymbol{p}}_{\varepsilon\delta\tau}$, $\boldsymbol{p}_{\varepsilon\delta\tau}$, $\overline{J}_{\varepsilon\delta\tau}$, $J_{\varepsilon\delta\tau}$, etc..

In terms of the piecewise constant and affine interpolants, cf. (25), the recursive system (22) can equivalently be reformulated:

$$\frac{\partial\varrho_{\varepsilon\delta\tau}}{\partial t} = \operatorname{div}\big(\delta|\nabla\underline{\varrho}_{\varepsilon\delta\tau}|^{r-2}\nabla\underline{\varrho}_{\varepsilon\delta\tau} - \mathcal{I}(\underline{\varrho}_{\varepsilon\delta\tau})\overline{\boldsymbol{p}}_{\varepsilon\delta\tau}\big) \quad\text{with } \overline{\boldsymbol{p}}_{\varepsilon\delta\tau} = \underline{\varrho}_{\varepsilon\delta\tau}\overline{\boldsymbol{v}}_{\varepsilon\delta\tau}\,, \tag{26a}$$

$$\begin{aligned}\frac{\partial\boldsymbol{p}_{\varepsilon\delta\tau}}{\partial t} = {}& \operatorname{div}\Big(\overline{\boldsymbol{D}}_{\varepsilon\delta\tau} - \mathcal{I}(\underline{\varrho}_{\varepsilon\delta\tau})\overline{\boldsymbol{p}}_{\varepsilon\delta\tau}\otimes\overline{\boldsymbol{v}}_{\varepsilon\delta\tau}\Big) - \nabla\overline{p}_{\varepsilon\delta\tau} - \big(\underline{\varrho}_{\varepsilon\delta\tau}+R\,\underline{c}_{\varepsilon\delta\tau}\big)\nabla V\\ & - \varepsilon|\overline{\boldsymbol{v}}_{\varepsilon\delta\tau}|^{q-2}\overline{\boldsymbol{v}}_{\varepsilon\delta\tau} - \delta|\nabla\underline{\varrho}_{\varepsilon\delta\tau}|^{r-2}(\nabla\overline{\boldsymbol{v}}_{\varepsilon\delta\tau})\nabla\underline{\varrho}_{\varepsilon\delta\tau}\,,\end{aligned}$$
$$\text{where } \overline{p}_{\varepsilon\delta\tau} = \underline{c}_{\varepsilon\delta\tau}\varphi'_c(\overline{J}_{\varepsilon\delta\tau},\overline{\chi}_{\varepsilon\delta\tau},\underline{c}_{\varepsilon\delta\tau}) - \overline{J}_{\varepsilon\delta\tau}\varphi'_J(\overline{J}_{\varepsilon\delta\tau},\overline{\chi}_{\varepsilon\delta\tau},\underline{c}_{\varepsilon\delta\tau}) - \varphi(\overline{J}_{\varepsilon\delta\tau},\overline{\chi}_{\varepsilon\delta\tau},\underline{c}_{\varepsilon\delta\tau})$$
$$\text{and}\quad \overline{\boldsymbol{D}}_{\varepsilon\delta\tau} = \mathbb{D}(\overline{p}_{\varepsilon\delta\tau},\overline{\chi}_{\varepsilon\delta\tau},\underline{c}_{\varepsilon\delta\tau},\boldsymbol{\varepsilon}(\overline{\boldsymbol{v}}_{\varepsilon\delta\tau}))\boldsymbol{\varepsilon}(\overline{\boldsymbol{v}}_{\varepsilon\delta\tau}) - \operatorname{div}\big(\nu\big|\nabla^2\overline{\boldsymbol{v}}_{\varepsilon\delta\tau}\big|^{q-2}\nabla^2\overline{\boldsymbol{v}}_{\varepsilon\delta\tau}\big)\,, \tag{26b}$$

$$\frac{\partial J_{\varepsilon\delta\tau}}{\partial t} = (\operatorname{div}\overline{\boldsymbol{v}}_{\varepsilon\delta\tau})\overline{J}_{\varepsilon\delta\tau} - \overline{\boldsymbol{v}}_{\varepsilon\delta\tau}\cdot\nabla\overline{J}_{\varepsilon\delta\tau}\,, \tag{26c}$$

$$\frac{\partial\chi_{\varepsilon\delta\tau}}{\partial t} = -(\overline{\boldsymbol{v}}_{\varepsilon\delta\tau}\cdot\nabla)\overline{\chi}_{\varepsilon\delta\tau}\,, \tag{26d}$$

$$\begin{aligned}\frac{\partial c_{\varepsilon\delta\tau}}{\partial t} = {}& \operatorname{div}\big(\overline{m}_{\varepsilon\delta\tau}\nabla\overline{\mu}_{\varepsilon\delta\tau} - \underline{c}_{\varepsilon\delta\tau}\overline{\boldsymbol{v}}_{\varepsilon\delta\tau}\big) + f(\overline{\chi}_{\varepsilon\delta\tau},\underline{c}_{\varepsilon\delta\tau})\\ & \text{with } \overline{\mu}_{\varepsilon\delta\tau} = \varphi'_c(\overline{J}_{\varepsilon\delta\tau},\overline{\chi}_{\varepsilon\delta\tau},\underline{c}_{\varepsilon\delta\tau}) + RV \text{ and } \overline{m}_{\varepsilon\delta\tau} = m(\overline{J}_{\varepsilon\delta\tau},\overline{\chi}_{\varepsilon\delta\tau},\underline{c}_{\varepsilon\delta\tau})\end{aligned} \tag{26e}$$

together with the respective boundary and initial conditions (13), (21), and (23) formulated in terms of the interpolants.

Proposition 3.2 (Stability and convergence of the discrete scheme (22))**.** *Let the assumptions (24) hold true. Then:*

(i) *For all $\varepsilon,\delta>0$, for all $\tau>0$ with $T/\tau\in\mathbb{N}$, for all $k\in\{1,\dots,T/\tau\}$ the time-discrete scheme (22) possesses a solution $(\varrho_{\varepsilon\delta\tau},\boldsymbol{p}_{\varepsilon\delta\tau},J_{\varepsilon\delta\tau},\chi_{\varepsilon\delta\tau},c_{\varepsilon\delta\tau})$, and thus it yields also $\boldsymbol{v}_{\varepsilon\delta\tau}$. Moreover, these solutions are stable with respect to $\tau>0$ (in the spaces specified later within the proof).*

(ii) *For all $\varepsilon,\delta>0$ fixed, there is a subsequence (not relabelled) of solutions $(\varrho_{\varepsilon\delta\tau},\boldsymbol{v}_{\varepsilon\delta\tau},J_{\varepsilon\delta\tau},\chi_{\varepsilon\delta\tau},c_{\varepsilon\delta\tau})_{\tau>0}$ which converges for $\tau\to0$ to a limit (in the topology specified within the proof) and every such a limit solves the initial-boundary-value problem for the system (19) in a weak sense.*

(iii) *Furthermore, as $\delta\to0$ and $\varepsilon\to0$ successively, the solutions obtained in (ii) converge (in terms of subsequences in the topology specified in the proof) to a weak solution $(\varrho,\boldsymbol{v},J,\chi,c)$ of (12) in the sense of Definition 3.1. In particular, (12) has at least one weak solution such that also the energy-dissipation balance (15) integrated over the time interval $[0,t]$ holds for any $t\in I$.*

Sketch of the proof. For clarity, we divide the proof into five steps. Some arguments are only sketched here, while referring to [31, Sec. 2.4], where a similar regularized time discretization of the subsystem (12a-c) without c and μ was studied by quite a similar arguments.

Step 1: Formal a-priori estimates and the choice of $\rho_{\max}$. We use (formally at this point) the energy-dissipation balance (15) together with the information $\varrho\geq0$ and $c\geq0$, which will be justified in Step 2. Treating the gravitational loading as in (31) below, we obtain, thanks to assumptions (24d), the formal a-priori bounds $\|\boldsymbol{\varepsilon}(\boldsymbol{v})\|_{L^2(I\times\Omega;\mathbb{R}^{d\times d})}\leq C$ and $\|\nabla^2\boldsymbol{v}\|_{L^q(I\times\Omega;\mathbb{R}^{d\times d\times d})}\leq C$.

This a-priori regularity of the velocity field together with the regularity of the initial datum $\varrho_0\in W^{1,r}(\Omega)$ in (24h) provides the the a-priori bound $\|\varrho\|_{L^\infty(I;W^{1,r}(\Omega))}\leq C_r$ from transport equation (1a), which suggests to put $\rho_{\max}>N_rC_r$ with N_r denoting the norm of the embedding $W^{1,r}(\Omega)\subset L^\infty(\Omega)$ for $r>d$. For details see [29, Lemma 5.1].

Step 2: Basic stability of the scheme (22) and first a-priori estimates. The energetics behind (22) can be revealed by the test of (22b) by $\boldsymbol{v}^k_{\varepsilon\delta\tau}$ and of (22e) by $\mu^k_{\varepsilon\delta\tau}$. The manipulation with the inertial part is quite technical and we refer to [31]; here the joint convexity of the mapping $(\boldsymbol{p},\varrho)\mapsto|\boldsymbol{p}|^2/\varrho$ on $(0,+\infty)\times\mathbb{R}^d$ is exploited and the test of (22a) by $|\boldsymbol{v}^k_{\varepsilon\delta\tau}|^2/2$. This last test also leads to the cancellation of the regularizing δ-terms in (22a) and (22b).

For the pressure term in (22), we calculate

$$\begin{aligned}\int_\Omega\nabla p^k_{\varepsilon\delta\tau}\cdot\boldsymbol{v}^k_{\varepsilon\delta\tau}\,\mathrm{d}\boldsymbol{x}&=\int_\Gamma p^k_{\varepsilon\delta\tau}\ \underbrace{\boldsymbol{v}^k_{\varepsilon\delta\tau}\cdot\boldsymbol{n}}_{=0}\ \mathrm{d}S-\int_\Omega p^k_{\varepsilon\delta\tau}\operatorname{div}\boldsymbol{v}^k_{\varepsilon\delta\tau}\,\mathrm{d}\boldsymbol{x}\\&=\int_\Omega\Big(J^k_{\varepsilon\delta\tau}\varphi'_J(J^k_{\varepsilon\delta\tau},\chi^k_{\varepsilon\delta\tau},c^k_{\varepsilon\delta\tau})-c^k_{\varepsilon\delta\tau}\varphi'_c(J^k_{\varepsilon\delta\tau},\chi^k_{\varepsilon\delta\tau},c^k_{\varepsilon\delta\tau})+\varphi(J^k_{\varepsilon\delta\tau},\chi^k_{\varepsilon\delta\tau},c^k_{\varepsilon\delta\tau})\Big)\operatorname{div}\boldsymbol{v}^k_{\varepsilon\delta\tau}\,\mathrm{d}\boldsymbol{x}\,.\end{aligned}\tag{27}$$

Moreover, when testing the transport equations (22c)–(22d) by the corresponding partial derivatives of the actual stored energy $\varphi'_\alpha(J^k_{\varepsilon\delta\tau},\chi^k_{\varepsilon\delta\tau},c^k_{\varepsilon\delta\tau})$ for $\alpha\in\{J,\chi\}$ and (22e) by $\mu^k_{\varepsilon\delta\tau}$, the convective terms in (22c)–(22e) can be summed up and a subsequent application of Green's formula yields

$$\begin{aligned}&\int_\Omega\Big(\varphi'_J(J^k_{\varepsilon\delta\tau},\chi^k_{\varepsilon\delta\tau},c^k_{\varepsilon\delta\tau})(\boldsymbol{v}^k_{\varepsilon\delta\tau}\cdot\nabla J^k_{\varepsilon\delta\tau})+\varphi'_\chi(J^k_{\varepsilon\delta\tau},\chi^k_{\varepsilon\delta\tau},c^k_{\varepsilon\delta\tau})(\boldsymbol{v}^k_{\varepsilon\delta\tau}\cdot\nabla\chi^k_{\varepsilon\delta\tau})\\&\qquad+\varphi'_c(J^k_{\varepsilon\delta\tau},\chi^k_{\varepsilon\delta\tau},c^k_{\varepsilon\delta\tau})(\boldsymbol{v}^k_{\varepsilon\delta\tau}\cdot\nabla c^k_{\varepsilon\delta\tau})\Big)\,\mathrm{d}\boldsymbol{x}=\int_\Omega\nabla\varphi(J^k_{\varepsilon\delta\tau},\chi^k_{\varepsilon\delta\tau},c^k_{\varepsilon\delta\tau})\cdot\boldsymbol{v}^k_{\varepsilon\delta\tau}\,\mathrm{d}\boldsymbol{x}\\&=\int_\Gamma\varphi(J^k_{\varepsilon\delta\tau},\chi^k_{\varepsilon\delta\tau},c^k_{\varepsilon\delta\tau})\ \underbrace{\boldsymbol{v}^k_{\varepsilon\delta\tau}\cdot\boldsymbol{n}}_{=0}\ \mathrm{d}S-\int_\Omega\varphi(J^k_{\varepsilon\delta\tau},\chi^k_{\varepsilon\delta\tau},c^k_{\varepsilon\delta\tau})\operatorname{div}\boldsymbol{v}^k_{\varepsilon\delta\tau}\,\mathrm{d}\boldsymbol{x}\,,\end{aligned}\tag{28}$$

where the right-hand side of (28) also shows the actual stored energy with opposite sign as in (27).

The assumed convexity (24a) of the actual stored energy φ allows for the estimate

$$\begin{aligned}
&\int_\Omega \frac{\varphi(J^k_{\varepsilon\delta\tau},\chi^k_{\varepsilon\delta\tau},c^k_{\varepsilon\delta\tau})-\varphi(J^{k-1}_{\varepsilon\delta\tau},\chi^{k-1}_{\varepsilon\delta\tau},c^{k-1}_{\varepsilon\delta\tau})}{\tau}+R\frac{c^k_{\varepsilon\delta\tau}-c^{k-1}_{\varepsilon\delta\tau}}{\tau}V\,\mathrm{d}\boldsymbol{x}\\
&\quad\le\int_\Omega\bigg(\varphi'_J(J^k_{\varepsilon\delta\tau},\chi^k_{\varepsilon\delta\tau},c^k_{\varepsilon\delta\tau})\frac{J^k_{\varepsilon\delta\tau}-J^{k-1}_{\varepsilon\delta\tau}}{\tau}\\
&\qquad\qquad+\varphi'_\chi(J^k_{\varepsilon\delta\tau},\chi^k_{\varepsilon\delta\tau},c^k_{\varepsilon\delta\tau})\cdot\frac{\chi^k_{\varepsilon\delta\tau}-\chi^{k-1}_{\varepsilon\delta\tau}}{\tau}+\Big(\varphi'_c(J^k_{\varepsilon\delta\tau},\chi^k_{\varepsilon\delta\tau},c^k_{\varepsilon\delta\tau})+RV\Big)\frac{c^k_{\varepsilon\delta\tau}-c^{k-1}_{\varepsilon\delta\tau}}{\tau}\bigg)\,\mathrm{d}\boldsymbol{x}\\
&\quad\overset{(22c,d)}{=}\int_\Omega\bigg(\varphi'_J(J^k_{\varepsilon\delta\tau},\chi^k_{\varepsilon\delta\tau},c^k_{\varepsilon\delta\tau})\Big((\operatorname{div}\boldsymbol{v}^k_{\varepsilon\delta\tau})J^k_{\varepsilon\delta\tau}-\boldsymbol{v}^k_{\varepsilon\delta\tau}\cdot\nabla J^k_{\varepsilon\delta\tau}\Big)-\varphi'_\chi(J^k_{\varepsilon\delta\tau},\chi^k_{\varepsilon\delta\tau},c^k_{\varepsilon\delta\tau})\cdot\boldsymbol{v}^k_{\varepsilon\delta\tau}\cdot\nabla\chi^k_{\varepsilon\delta\tau}\\
&\qquad\qquad+\mu^k_{\varepsilon\delta\tau}\Big(\operatorname{div}\big(m^k_{\varepsilon\delta\tau}\nabla\mu^k_{\varepsilon\delta\tau}\big)-\boldsymbol{v}^k_{\varepsilon\delta\tau}\cdot\nabla c^k_{\varepsilon\delta\tau}-c^k_{\varepsilon\delta\tau}\operatorname{div}\boldsymbol{v}^k_{\varepsilon\delta\tau}+f(\chi^k_{\varepsilon\delta\tau},c^k_{\varepsilon\delta\tau})\Big)\bigg)\,\mathrm{d}\boldsymbol{x}\\
&\quad\overset{(28)}{=}\int_\Omega\bigg(\Big(J^k_{\varepsilon\delta\tau}\varphi'_J(J^k_{\varepsilon\delta\tau},\chi^k_{\varepsilon\delta\tau},c^k_{\varepsilon\delta\tau})+\varphi(J^k_{\varepsilon\delta\tau},\chi^k_{\varepsilon\delta\tau},c^k_{\varepsilon\delta\tau})-c^k_{\varepsilon\delta\tau}\mu^k_{\varepsilon\delta\tau}\Big)\operatorname{div}\boldsymbol{v}^k_{\varepsilon\delta\tau}\\
&\qquad\qquad-m^k_{\varepsilon\delta\tau}|\nabla\mu^k_{\varepsilon\delta\tau}|^2+\mu^k_{\varepsilon\delta\tau}f(\chi^k_{\varepsilon\delta\tau},c^k_{\varepsilon\delta\tau})\bigg)\,\mathrm{d}\boldsymbol{x}\\
&\quad\overset{(27)}{=}\int_\Omega\big(p^k_{\varepsilon\delta\tau}-Rc^k_{\varepsilon\delta\tau}V\big)\operatorname{div}\boldsymbol{v}^k_{\varepsilon\delta\tau}-m^k_{\varepsilon\delta\tau}|\nabla\mu^k_{\varepsilon\delta\tau}|^2+\mu^k_{\varepsilon\delta\tau}f(\chi^k_{\varepsilon\delta\tau},c^k_{\varepsilon\delta\tau})\,\mathrm{d}\boldsymbol{x}
\end{aligned}\tag{29}$$

with $m^k_{\varepsilon\delta\tau}=m(J^k_{\varepsilon\delta\tau},\chi^k_{\varepsilon\delta\tau},c^k_{\varepsilon\delta\tau})$. Notably the discrete analogue (5) would be here cumbersome because of the regularization/truncation of the continuity equation (22a) would now rise some higher-order terms in a discrete analogue of (6) which would be difficult to use for some estimates.

All the above arguments give the overall discrete energy-dissipation (im)balance

$$\begin{aligned}
&\int_\Omega\frac{|\boldsymbol{p}^k_{\varepsilon\delta\tau}|^2}{2\varrho^k_{\varepsilon\delta\tau}}+\varphi(J^k_{\varepsilon\delta\tau},\chi^k_{\varepsilon\delta\tau},c^k_{\varepsilon\delta\tau})+Rc^k_{\varepsilon\delta\tau}V\,\mathrm{d}\boldsymbol{x}\\
&+\sum_{l=1}^k\int_\Omega\tau\Big(\mathbb{D}(J^l_{\varepsilon\delta\tau},\chi^l_{\varepsilon\delta\tau},c^l_{\varepsilon\delta\tau},\boldsymbol{\varepsilon}(\boldsymbol{v}^l_{\varepsilon\delta\tau}))|\boldsymbol{\varepsilon}(\boldsymbol{v}^l_{\varepsilon\delta\tau})|^2+m^l_{\varepsilon\delta\tau}|\nabla\mu^l_{\varepsilon\delta\tau}|^2+\nu|\nabla^2\boldsymbol{v}^l_{\varepsilon\delta\tau}|^q+\varepsilon|\boldsymbol{v}^l_{\varepsilon\delta\tau}|^q\Big)\,\mathrm{d}\boldsymbol{x}\\
&\qquad\le\int_\Omega\frac{|\boldsymbol{p}_0|^2}{2\varrho_0}+\varphi(J_0,\chi_0,c_0)+Rc_0V\,\mathrm{d}\boldsymbol{x}+\tau\sum_{l=1}^k\int_\Omega\mu^l_{\varepsilon\delta\tau}f(\chi^l_{\varepsilon\delta\tau},c^l_{\varepsilon\delta\tau})+\varrho^l_{\varepsilon\delta\tau}V\cdot\boldsymbol{v}^l_{\varepsilon\delta\tau}\,\mathrm{d}\boldsymbol{x}\,.
\end{aligned}\tag{30}$$

The last term can be estimated by the discrete Gronwall inequality as in [31, Formula (2.33)] while the left-hand-side term $\int_\Omega Rc^k_{\varepsilon\delta\tau}V\,\mathrm{d}\boldsymbol{x}$ is to be estimated "on the right-hand side" as

$$-\int_\Omega Rc^k_{\varepsilon\delta\tau}V\,\mathrm{d}\boldsymbol{x}\le\sup|V|\int_\Omega Rc^k_{\varepsilon\delta\tau}\,\mathrm{d}\boldsymbol{x}\le\sup|V|\bigg(\int_\Omega Rc_0\,\mathrm{d}\boldsymbol{x}+k\tau\sup|f|\bigg)\,,\tag{31}$$

where we used that the total mass is constant due to the discrete continuity equation (22a) and the boundary condition $\boldsymbol{v}^l_{\varepsilon\delta\tau}\cdot\boldsymbol{n}=0$ on Γ and similarly the total diffusant content is controlled exclusively by the diffusant supply f due to the discrete diffusion equation (22b) and the boundary conditions $\boldsymbol{v}^l_{\varepsilon\delta\tau}\cdot\boldsymbol{n}=0$ and $\mu^l_{\varepsilon\delta\tau}\cdot\boldsymbol{n}=0$. The term of the right-hand side $f(\chi^l_{\varepsilon\delta\tau},c^l_{\varepsilon\delta\tau})\,\mu^l_{\varepsilon\delta\tau}$ can be estimated by using (24b) and (24f) as

$$\int_\Omega|f(\chi^l_{\varepsilon\delta\tau},c^l_{\varepsilon\delta\tau})\,\mu^l_{\varepsilon\delta\tau}|\,\mathrm{d}\boldsymbol{x}\le C\bigg(1+\int_\Omega J^l_{\varepsilon\delta\tau}+(c^l_{\varepsilon\delta\tau})^2\,\mathrm{d}\boldsymbol{x}\bigg)\le\frac{C}{\eta}\bigg(\frac{1}{\eta^2}+\frac{1}{\eta}\int_\Omega\varphi(J^l_{\varepsilon\delta\tau},\chi^l_{\varepsilon\delta\tau},c^l_{\varepsilon\delta\tau})\,\mathrm{d}\boldsymbol{x}\bigg)\,.\tag{32}$$

For the handling regularizing force in (26b), we refer to [31, Formula (2.29)].

The estimates (31) and (32) can be treated by the discrete Gronwall inequality. Here, taking into account the coercivity assumption (24b), we should note that the coefficients on the right-hand sides of (31) and (32) are constant so that the discrete Gronwall inequality indeed holds for $\tau>0$ sufficiently small, depending on M, R,

and V. Thus, from (30), we can read the estimates

$$\left\|\frac{\overline{\boldsymbol{p}}_{\varepsilon\delta\tau}}{\sqrt{\overline{\varrho}_{\varepsilon\delta\tau}}}\right\|_{L^\infty(I;L^2(\Omega;\mathbb{R}^d))}\leq C \quad\text{and}\quad \|\overline{\boldsymbol{v}}_{\varepsilon\delta\tau}\|_{L^q(I\times\Omega;\mathbb{R}^d)}\leq\frac{C}{\sqrt[q]{\varepsilon}}\,, \tag{33a}$$

$$\|\boldsymbol{\varepsilon}(\overline{\boldsymbol{v}}_{\varepsilon\delta\tau})\|_{L^2(I\times\Omega;\mathbb{R}^{d\times d})}\leq C \quad\text{and}\quad \|\nabla^2\overline{\boldsymbol{v}}_{\varepsilon\delta\tau}\|_{L^q(I\times\Omega;\mathbb{R}^{d\times d\times d})}\leq C\,, \tag{33b}$$

$$\left\|\varphi(\overline{J}_{\varepsilon\delta\tau},\overline{\chi}_{\varepsilon\delta\tau},\overline{c}_{\varepsilon\delta\tau})\right\|_{L^\infty(I;L^1(\Omega))}\leq C\,, \tag{33c}$$

$$\left\|\overline{m}_{\varepsilon\delta\tau}|\nabla\overline{\mu}_{\varepsilon\delta\tau}|^2\right\|_{L^1(I\times\Omega)}\leq C \quad\text{with}\quad \overline{m}_{\varepsilon\delta\tau}=m(\overline{J}_{\varepsilon\delta\tau},\overline{\chi}_{\varepsilon\delta\tau},\overline{c}_{\varepsilon\delta\tau})\,. \tag{33d}$$

By the coercivity and growth (24b) of φ, the last estimate implies

$$\|\overline{J}_{\varepsilon\delta\tau}\|_{L^\infty(I;L^1(\Omega))}\leq C \quad\text{and}\quad \|\overline{c}_{\varepsilon\delta\tau}\|_{L^\infty(I;L^2(\Omega))}\leq C. \tag{33e}$$

Then, from the former estimate in (33a) and from $\overline{\varrho}_{\varepsilon\delta\tau}\leq\rho_{\max}+1$, we have also

$$\begin{aligned}\|\overline{\boldsymbol{p}}_{\varepsilon\delta\tau}\|_{L^\infty(I;L^1(\Omega;\mathbb{R}^d))}&\leq\left\|\sqrt{\overline{\varrho}_{\varepsilon\delta\tau}}\right\|_{L^\infty(I;L^2(\Omega;\mathbb{R}^d))}\left\|\frac{\overline{\boldsymbol{p}}_{\varepsilon\delta\tau}}{\sqrt{\overline{\varrho}_{\varepsilon\delta\tau}}}\right\|_{L^\infty(I;L^2(\Omega;\mathbb{R}^d))}\\&=\mathrm{meas}(\Omega)(\rho_{\max}+1)\left\|\frac{\overline{\boldsymbol{p}}_{\varepsilon\delta\tau}}{\sqrt{\overline{\varrho}_{\varepsilon\delta\tau}}}\right\|_{L^\infty(I;L^2(\Omega;\mathbb{R}^d))}\leq C\end{aligned} \tag{33f}$$

with C here and below denoting a generic constant; it is important that C in these estimates (33) is independent of δ and of ε.

It is not difficult to see that, for a sufficiently small $\tau>0$, we have $c^k_{\varepsilon\delta\tau}\geq 0$ a.e. when $c_0\geq 0$ a.e.: indeed, it suffices to test (22d) by $(c^k_{\varepsilon\delta\tau})^-:=\max(0,-c^k_{\varepsilon\delta\tau})$. Due to (24g) and relying on the convexity of $(\cdot)^-$, we obtain

$$\begin{aligned}&\int_\Omega\frac{((c^k_{\varepsilon\delta\tau})^-)^2-((c^{k-1}_{\varepsilon\delta\tau})^-)^2}{2\tau}\,\mathrm{d}\boldsymbol{x}\\&\leq\int_\Omega f(\chi^k_{\varepsilon\delta\tau},c^k_{\varepsilon\delta\tau})(c^k_{\varepsilon\delta\tau})^-\,-\Big(m(J^k_{\varepsilon\delta\tau},\chi^k_{\varepsilon\delta\tau},c^k_{\varepsilon\delta\tau})\nabla\mu^k_{\varepsilon\delta\tau}-c^k_{\varepsilon\delta\tau}\boldsymbol{v}^k_{\varepsilon\delta\tau}\Big)\cdot\nabla(c^k_{\varepsilon\delta\tau})^-\,\mathrm{d}\boldsymbol{x}\\&=-\frac{1}{2}\int_\Omega((c^k_{\varepsilon\delta\tau})^-)^2\mathrm{div}\,\boldsymbol{v}^k_{\varepsilon\delta\tau}\,\mathrm{d}\boldsymbol{x}\,,\end{aligned}$$

where we used the Green formula for the convective term $c\boldsymbol{v}\cdot\nabla c^-=c^-\boldsymbol{v}\cdot\nabla c^-$ and that $m(J,\chi,c)\nabla c^-=0$ as well as $f(\chi,c)c^-=0$. Having the estimate (33b) at disposal, we can use the discrete Gronwall inequality like (36)–(37) below to see $\int_\Omega(c^k_{\varepsilon\delta\tau})^-\,\mathrm{d}\boldsymbol{x}=0$ for each $k=1,2,...$

Notably, even $c^k_{\varepsilon\delta\tau}>0$ a.e. on Ω when $c^{k-1}_{\varepsilon\delta\tau}>0$ a.e. This can be seen by a contradiction argument: assuming $c^{k-1}_{\varepsilon\delta\tau}>0$ on $\bar\Omega$ and the minimum of a (momentarily smooth) solution $c^k_{\varepsilon\delta\tau}$ is attained at some $\boldsymbol{x}\in\Omega$ and $c^k_{\varepsilon\delta\tau}(\boldsymbol{x})=0$, so that $c^k_{\varepsilon\delta\tau}(\boldsymbol{x})-c^{k-1}_{\varepsilon\delta\tau}(\boldsymbol{x})<0$ and $\nabla c^k_{\varepsilon\delta\tau}(\boldsymbol{x})=\boldsymbol{0}$. Taking into account also that $m(J,\chi,c)=0$ and $m'_J(J,\chi,c)=m'_\chi(J,\chi,c)=0$ for $c=0$, cf. (24g), we have that

$$\begin{aligned}&\mathrm{div}\Big(m^k_{\varepsilon\delta\tau}(\boldsymbol{x})\nabla\mu^k_{\varepsilon\delta\tau}(\boldsymbol{x})\Big)=m^k_{\varepsilon\delta\tau}(\boldsymbol{x})\Delta\mu^k_{\varepsilon\delta\tau}(\boldsymbol{x})+\Big(m'_J(J^k_{\varepsilon\delta\tau}(\boldsymbol{x}),\chi^k_{\varepsilon\delta\tau}(\boldsymbol{x}),c^k_{\varepsilon\delta\tau}(\boldsymbol{x}))\nabla J^k_{\varepsilon\delta\tau}(\boldsymbol{x})\\&+m'_\chi(J^k_{\varepsilon\delta\tau}(\boldsymbol{x}),\chi^k_{\varepsilon\delta\tau}(\boldsymbol{x}),c^k_{\varepsilon\delta\tau}(\boldsymbol{x}))\nabla\chi^k_{\varepsilon\delta\tau}(\boldsymbol{x})\\&+m'_c(J^k_{\varepsilon\delta\tau}(\boldsymbol{x}),\chi^k_{\varepsilon\delta\tau}(\boldsymbol{x}),c^k_{\varepsilon\delta\tau}(\boldsymbol{x}))\nabla c^k_{\varepsilon\delta\tau}(\boldsymbol{x})\Big)\cdot\nabla\mu^k_{\varepsilon\delta\tau}(\boldsymbol{x})=0\,.\end{aligned}$$

Also, $\mathrm{div}(c^k_{\varepsilon\delta\tau}(\boldsymbol{x})\boldsymbol{v}^k_{\varepsilon\delta\tau}(\boldsymbol{x}))=c^k_{\varepsilon\delta\tau}(\boldsymbol{x})\mathrm{div}\,\boldsymbol{v}^k_{\varepsilon\delta\tau}(\boldsymbol{x})+\boldsymbol{v}^k_{\varepsilon\delta\tau}(\boldsymbol{x})\cdot\nabla c^k_{\varepsilon\delta\tau}(\boldsymbol{x})=0$ and $f(\chi^k_{\varepsilon\delta\tau}(\boldsymbol{x}),c^k_{\varepsilon\delta\tau}(\boldsymbol{x}))=0$. Altogether, from (22e) written at $\boldsymbol{x}$ in the form

$$c^k_{\varepsilon\delta\tau}(\boldsymbol{x})-c^{k-1}_{\varepsilon\delta\tau}(\boldsymbol{x})=\tau\mathrm{div}\left(m^k_{\varepsilon\delta\tau}(\boldsymbol{x})\nabla\mu^k_{\varepsilon\delta\tau}(\boldsymbol{x})-c^k_{\varepsilon\delta\tau}(\boldsymbol{x})\boldsymbol{v}^k_{\varepsilon\delta\tau}(\boldsymbol{x})\right)+\tau f(\chi^k_{\varepsilon\delta\tau}(\boldsymbol{x}),c^k_{\varepsilon\delta\tau}(\boldsymbol{x}))=0,$$

we obtain the contradiction showing that $c^k_{\varepsilon\delta\tau}(\boldsymbol{x})>0$.

Step 3: Estimates of $\nabla J_{\varepsilon\delta\tau}$ *and* $\nabla c_{\varepsilon\delta\tau}$. The estimates (33b) together with the regularity of the initial condition $J_0 \in W^{1,r}(\Omega)$ as assumed in (24h) allows also to obtain estimate of $\nabla \overline{J}_{\varepsilon\delta\tau}$. To this goal, we first need an estimate of $\overline{J}_{\varepsilon\delta\tau}$ in $L^\infty(I;L^s(\Omega))$ with a sufficiently big s by testing (22c) by $|J^k_{\varepsilon\delta\tau}|^{s-2}J^k_{\varepsilon\delta\tau}$. We use the following calculus with the boundary condition $\boldsymbol{v}^k_{\varepsilon\delta\tau}\cdot\boldsymbol{n}=0$:

$$\begin{aligned}\int_\Omega (\boldsymbol{v}^k_{\varepsilon\delta\tau}\cdot\nabla J^k_{\varepsilon\delta\tau})\,|J^k_{\varepsilon\delta\tau}|^{s-2}J^k_{\varepsilon\delta\tau}\,\mathrm{d}\boldsymbol{x} &\overset{\text{Green formula}}{=} \int_\Gamma |J^k_{\varepsilon\delta\tau}|^s(\boldsymbol{v}^k_{\varepsilon\delta\tau}\cdot\boldsymbol{n})\,\mathrm{d}S\\ -\int_\Omega (s-1)|J^k_{\varepsilon\delta\tau}|^{s-2}J^k_{\varepsilon\delta\tau}(\boldsymbol{v}^k_{\varepsilon\delta\tau}\cdot\nabla J^k_{\varepsilon\delta\tau}) + (\operatorname{div}\boldsymbol{v}^k_{\varepsilon\delta\tau})|J^k_{\varepsilon\delta\tau}|^s\mathrm{d}\boldsymbol{x} &= -\frac{1}{s}\int_\Omega (\operatorname{div}\boldsymbol{v}^k_{\varepsilon\delta\tau})|J^k_{\varepsilon\delta\tau}|^s\mathrm{d}\boldsymbol{x}\,,\end{aligned} \tag{34}$$

we obtain

$$\begin{aligned}\frac{1}{s}\int_\Omega \frac{|J^k_{\varepsilon\delta\tau}|^s-|J^{k-1}_{\varepsilon\delta\tau}|^s}{\tau}\,\mathrm{d}\boldsymbol{x} &\le \int_\Omega \frac{1}{s}(\operatorname{div}\boldsymbol{v}^k_{\varepsilon\delta\tau})|J^k_{\varepsilon\delta\tau}|^s - (\boldsymbol{v}^k_{\varepsilon\delta\tau}\cdot\nabla J^k_{\varepsilon\delta\tau})|J^k_{\varepsilon\delta\tau}|^{s-2}J^k_{\varepsilon\delta\tau}\,\mathrm{d}\boldsymbol{x}\\ &\le \Big(1+\frac{1}{s}\Big)\,\|\operatorname{div}\boldsymbol{v}^k_{\varepsilon\delta\tau}\|_{L^\infty(\Omega)}\int_\Omega |J^k_{\varepsilon\delta\tau}|^s\,\mathrm{d}\boldsymbol{x}\,.\end{aligned} \tag{35}$$

Now we can use the discrete Gronwall inequality, which however needs the uniform bound of the coefficient $\|\operatorname{div}\boldsymbol{v}^k_{\varepsilon\delta\tau}\|_{L^q(\Omega)}$, specifically

$$\inf_{0<\tau\le\tau_0}\ \tau\,\Big(\max_{k=1,\dots,T/\tau}\|\operatorname{div}\boldsymbol{v}^k_{\varepsilon\delta\tau}\|_{L^q(\Omega)}\Big)<1\,. \tag{36}$$

It is important that the already obtained estimates in (33b) imply

$$\exists C_q<\infty\ \forall\tau>0:\qquad \tau\sum_{k=1}^{T/\tau}\|\operatorname{div}\boldsymbol{v}^k_{\varepsilon\delta\tau}\|^q_{L^\infty(\Omega)}\le C_q\,; \tag{37}$$

here the embedding $W^{1,q}(\Omega)\subset L^\infty(\Omega)$ has been used.

The worst scenario which gives the largest $\|\operatorname{div}\boldsymbol{v}^k_{\varepsilon\delta\tau}\|_{L^\infty(\Omega)}$ under the condition (36) is that all $\boldsymbol{v}^k_\tau$ are zero except one, say with $k=1$, for which $\tau\|\operatorname{div}\boldsymbol{v}^1_\tau\|^q_{L^\infty(\Omega)}=C_q$. Then $\max_{k=1,\dots,T/\tau}\|\operatorname{div}\boldsymbol{v}^k_{\varepsilon\delta\tau}\|_{L^\infty(\Omega)}=(C_q/\tau)^{1/q}$. Since $q>1$ is assumed, (36) is satisfied for sufficiently small $\tau_0>0$. Thus we obtain the estimate

$$\|\,\overline{J}_{\varepsilon\delta\tau}\|_{L^\infty(I;L^s(\Omega))}\le C_s\,. \tag{38}$$

Now we can test (22c) by the r-Laplacian $-\operatorname{div}(|\nabla J^k_{\varepsilon\delta\tau}|^{r-2}\nabla J^k_{\varepsilon\delta\tau})$. This means the application of the ∇-operator to (22c) and then the test by $|\nabla J^k_{\varepsilon\delta\tau}|^{r-2}\nabla J^k_{\varepsilon\delta\tau}$. For the convective term, we use the calculus again exploiting the Green formula:

$$\begin{aligned}&\int_\Omega \nabla\big(\boldsymbol{v}^k_{\varepsilon\delta\tau}\cdot\nabla J^k_{\varepsilon\delta\tau}\big):|\nabla J^k_{\varepsilon\delta\tau}|^{r-2}\nabla J^k_{\varepsilon\delta\tau}\,\mathrm{d}\boldsymbol{x}\\ &=\int_\Omega |\nabla J^k_{\varepsilon\delta\tau}|^{r-2}(\nabla J^k_{\varepsilon\delta\tau}\otimes\nabla J^k_{\varepsilon\delta\tau}):\boldsymbol{\varepsilon}(\boldsymbol{v}^k_{\varepsilon\delta\tau}) + (\boldsymbol{v}^k_{\varepsilon\delta\tau}\cdot\nabla)\nabla J^k_{\varepsilon\delta\tau}\cdot|\nabla J^k_{\varepsilon\delta\tau}|^{r-2}\nabla J^k_{\varepsilon\delta\tau}\,\mathrm{d}\boldsymbol{x}\\ &=\int_\Gamma |\nabla J^k_{\varepsilon\delta\tau}|^r\ \underbrace{\boldsymbol{v}^k_{\varepsilon\delta\tau}\cdot\boldsymbol{n}}_{=0}\ \mathrm{d}S+\int_\Omega\Big(|\nabla J^k_{\varepsilon\delta\tau}|^{r-2}(\nabla J^k_{\varepsilon\delta\tau}\otimes\nabla J^k_{\varepsilon\delta\tau}):\boldsymbol{\varepsilon}(\boldsymbol{v}^k_{\varepsilon\delta\tau})\\ &\qquad\qquad -(\operatorname{div}\boldsymbol{v}^k_{\varepsilon\delta\tau})|\nabla J^k_{\varepsilon\delta\tau}|^r-(r-1)|\nabla J^k_{\varepsilon\delta\tau}|^{r-2}\nabla J^k_{\varepsilon\delta\tau}\cdot(\boldsymbol{v}^k_{\varepsilon\delta\tau}\cdot\nabla)\nabla J^k_{\varepsilon\delta\tau}\Big)\,\mathrm{d}\boldsymbol{x}\\ &=\int_\Omega |\nabla J^k_{\varepsilon\delta\tau}|^{r-2}(\nabla J^k_{\varepsilon\delta\tau}\otimes\nabla J^k_{\varepsilon\delta\tau}):\boldsymbol{\varepsilon}(\boldsymbol{v}^k_{\varepsilon\delta\tau})-\frac{1}{r}(\operatorname{div}\boldsymbol{v}^k_{\varepsilon\delta\tau})|\nabla J^k_{\varepsilon\delta\tau}|^r\,\mathrm{d}\boldsymbol{x}\,.\end{aligned} \tag{39}$$

Moreover, the term $(\operatorname{div}\boldsymbol{v}^k_{\varepsilon\delta\tau})J^k_{\varepsilon\delta\tau}$ gives under this test:

$$\begin{aligned}&\int_\Omega \nabla\big((\operatorname{div}\boldsymbol{v}^k_{\varepsilon\delta\tau})J^k_{\varepsilon\delta\tau}\big)\cdot|\nabla J^k_{\varepsilon\delta\tau}|^{r-2}\nabla J^k_{\varepsilon\delta\tau}\,\mathrm{d}\boldsymbol{x}\\ &\quad=\int_\Omega(\operatorname{div}\boldsymbol{v}^k_{\varepsilon\delta\tau})|\nabla J^k_{\varepsilon\delta\tau}|^r+J^k_{\varepsilon\delta\tau}|\nabla J^k_{\varepsilon\delta\tau}|^{r-2}\nabla J^k_{\varepsilon\delta\tau}\cdot\nabla(\operatorname{div}\boldsymbol{v}^k_{\varepsilon\delta\tau})\,\mathrm{d}\boldsymbol{x}\,,\end{aligned}$$

where the last term is to be estimated by the Hölder inequality as

$$\left|\int_\Omega J^k_{\varepsilon\delta\tau}|\nabla J^k_{\varepsilon\delta\tau}|^{r-2}\nabla J^k_{\varepsilon\delta\tau}\cdot\nabla(\operatorname{div}\boldsymbol{v}^k_{\varepsilon\delta\tau})\,\mathrm{d}\boldsymbol{x}\right| \leq C_{r,s}\Big(1+\|\nabla(\operatorname{div}\boldsymbol{v}^k_{\varepsilon\delta\tau})\|^q_{L^q(\Omega;\mathbb{R}^d)}+\|J^k_{\varepsilon\delta\tau}\|^s_{L^s(\Omega)}+\|\nabla J^k_{\varepsilon\delta\tau}\|^r_{L^r(\Omega;\mathbb{R}^d)}\Big) \tag{40}$$

provided $s\geq rq/(q-r)$; here we need the condition $q>r$. Altogether, by (39) and (40) and by using also (38) with this choice of s, we obtain the estimate of the type

$$\frac{1}{r}\int_\Omega\frac{|\nabla J^k_{\varepsilon\delta\tau}|^r-|\nabla J^{k-1}_{\varepsilon\delta\tau}|^r}{\tau}\,\mathrm{d}\boldsymbol{x}\leq C\bigg(1+\Big(1+\|\boldsymbol{\varepsilon}(\boldsymbol{v}^k_{\varepsilon\delta\tau})\|_{W^{1,q}(\Omega;\mathbb{R}^{d\times d})}\Big)\|\nabla J^k_{\varepsilon\delta\tau}\|^r_{L^r(\Omega;\mathbb{R}^d)}\bigg)\,.$$

Using the discrete Gronwall inequality supported by similar arguments as used for (38), we obtain for sufficiently small τ's that

$$\|\overline{J}_{\varepsilon\delta\tau}\|_{L^\infty(I;W^{1,r}(\Omega))}\leq C_r\,. \tag{41}$$

The estimate (33c) in combination with the of $J\mapsto\varphi(J,c)$ to $+\infty$ for $J\to0+$ assumed in (24b) gives the boundedness of $\sup_{t\in I}\int_\Omega|\overline{J}_{\varepsilon\delta\tau}(t,\boldsymbol{x})|^{-s}\,\mathrm{d}\boldsymbol{x}\leq C$ uniform also in ε and δ. The estimate (41) with $r>d$ together with the sufficiently fast blowup with $s>rd/(r-d)$ as assumed in (24b) allows for usage Healey-Krömer's arguments [17] to obtain the estimate

$$\exists\,J_{\min}>0:\quad\inf_{(t,\boldsymbol{x})\in I\times\Omega}\overline{J}_{\varepsilon\delta\tau}(t,\boldsymbol{x})\geq J_{\min}\,. \tag{42}$$

This is a fine result exploiting also a certain regularity of the boundary Γ, namely the so-called cone property which is, in particular, satisfied for all Lipschitz domains; cf. also [19, Theorems 2.5.2–3].

Let us now turn to the estimation of $\nabla c_{\varepsilon\delta\tau}$. Since the mobility $m(J,c)$ naturally degenerates at $c=0$, we cannot read any information about $\nabla\mu$, neither for ∇c, directly from (30). For this reason, we still make a "non-physical" test of (22e) by $c^k_{\varepsilon\delta\tau}$. For the convective term, we use the calculus (34) now for $s=2$ and the boundary condition $\boldsymbol{v}\cdot\boldsymbol{n}=0$, *i.e.*

$$\int_\Omega\operatorname{div}(c^k_{\varepsilon\delta\tau}\boldsymbol{v}^k_{\varepsilon\delta\tau})\,c^k_{\varepsilon\delta\tau}\,\mathrm{d}\boldsymbol{x}\overset{\text{Green formula}}{=}-\int_\Omega(\boldsymbol{v}^k_{\varepsilon\delta\tau}\cdot\nabla c^k_{\varepsilon\delta\tau})\,c^k_{\varepsilon\delta\tau}\,\mathrm{d}\boldsymbol{x}\overset{\text{Green formula}}{=}\int_\Omega(\operatorname{div}\boldsymbol{v}^k_{\varepsilon\delta\tau})\frac{|c^k_{\varepsilon\delta\tau}|^2}{2}\,\mathrm{d}\boldsymbol{x}\,.$$

Exploiting the chain rule

$$\begin{aligned}m^k_{\varepsilon\delta\tau}\,\nabla\mu^k_{\varepsilon\delta\tau}\cdot\nabla c^k_{\varepsilon\delta\tau}&=m^k_{\varepsilon\delta\tau}\,\nabla\big(\varphi'_c(J^k_{\varepsilon\delta\tau},\chi^k_{\varepsilon\delta\tau},c^k_{\varepsilon\delta\tau})+RV\big)\cdot\nabla c^k_{\varepsilon\delta\tau}\\&=m^k_{\varepsilon\delta\tau}\,\varphi''_{cc}(J^k_{\varepsilon\delta\tau},\chi^k_{\varepsilon\delta\tau},c^k_{\varepsilon\delta\tau})|\nabla c^k_{\varepsilon\delta\tau}|^2+m^k_{\varepsilon\delta\tau}\,\big(\varphi''_{Jc}(J^k_{\varepsilon\delta\tau},\chi^k_{\varepsilon\delta\tau},c^k_{\varepsilon\delta\tau})\nabla J^k_{\varepsilon\delta\tau}+R\nabla V\big)\cdot\nabla c^k_{\varepsilon\delta\tau}\,,\end{aligned}$$

the test of (22e) by $c^k_{\varepsilon\delta\tau}$ yields

$$\begin{aligned}&\int_\Omega\frac{|c^k_{\varepsilon\delta\tau}|^2-|c^{k-1}_{\varepsilon\delta\tau}|^2}{2\tau}+\underbrace{m^k_{\varepsilon\delta\tau}\,\varphi''_{cc}(J^k_{\varepsilon\delta\tau},\chi^k_{\varepsilon\delta\tau},c^k_{\varepsilon\delta\tau})}_{\geq a_1>0}\,|\nabla c^k_{\varepsilon\delta\tau}|^2\,\mathrm{d}\boldsymbol{x}\\&\leq\int_\Omega c^k_{\varepsilon\delta\tau}f(J^k_{\varepsilon\delta\tau},\chi^k_{\varepsilon\delta\tau},c^k_{\varepsilon\delta\tau})-m^k_{\varepsilon\delta\tau}\,\big(\varphi''_{Jc}(J^k_{\varepsilon\delta\tau},\chi^k_{\varepsilon\delta\tau},c^k_{\varepsilon\delta\tau})\nabla J^k_{\varepsilon\delta\tau}+R\nabla V\big)\cdot\nabla c^k_{\varepsilon\delta\tau}-(\operatorname{div}\boldsymbol{v}^k_{\varepsilon\delta\tau})\frac{|c^k_{\varepsilon\delta\tau}|^2}{2}\,\mathrm{d}\boldsymbol{x}\\&\leq\int_\Omega1+J^k_{\varepsilon\delta\tau}+(c^k_{\varepsilon\delta\tau})^2+a_2\big(1+c^k_{\varepsilon\delta\tau}\big)|\nabla J^k_{\varepsilon\delta\tau}|\,|\nabla c^k_{\varepsilon\delta\tau}|-(\operatorname{div}\boldsymbol{v}^k_{\varepsilon\delta\tau})\frac{|c^k_{\varepsilon\delta\tau}|^2}{2}\,\mathrm{d}\boldsymbol{x}\,,\end{aligned}$$

where

$$\begin{aligned}a_1&=\inf_{J_{\min}\leq J\leq J_{\max},\ c,\chi\in(0,+\infty)}m(J,\chi,c)\,\varphi''_{cc}(J,\chi,c)\quad\text{and}\\a_2&=\sup_{J_{\min}\leq J\leq J_{\max},\ c,\chi\in(0,+\infty)}\frac{m(J,\chi,c)(|(\varphi''_{Jc}(J,\chi,c)|+R|V|)}{1+c}\,,\end{aligned}$$

with some $J_{\max} > \|\overline{J}_{\varepsilon\delta\tau}\|_{L^\infty(I\times\Omega)}$ which is finite due to (41) with $r > d$. Also the assumptions (24c) and (24f) have been used here. Relying on (33e) and (41), by the Hölder inequality we estimate

$$\begin{aligned}\int_\Omega a_2\big(1+c^k_{\varepsilon\delta\tau}\big)|\nabla J^k_{\varepsilon\delta\tau}|\,|\nabla c^k_{\varepsilon\delta\tau}|\,\mathrm{d}\boldsymbol{x} &\le C_r\Big(1+\big\|c^k_{\varepsilon\delta\tau}\big\|_{L^6(\Omega)}\Big)\|\nabla J^k_{\varepsilon\delta\tau}\|_{L^r(\Omega;\mathbb{R}^d)}\|\nabla c^k_{\varepsilon\delta\tau}\|_{L^2(\Omega;\mathbb{R}^d)}\\ &\le C_r\|\nabla J^k_{\varepsilon\delta\tau}\|_{L^r(\Omega;\mathbb{R}^d)}\Big(1+N+N\|c^k_{\varepsilon\delta\tau}\|_{L^2(\Omega)}\Big)\Big(1+\|\nabla c^k_{\varepsilon\delta\tau}\|^2_{L^2(\Omega;\mathbb{R}^d)}\Big)\,,\end{aligned} \tag{43}$$

where we used the embedding $H^1(\Omega)\subset L^6(\Omega)$ implying the inequality $\|\cdot\|_{L^6(\Omega)}\le N(\|\cdot\|_{L^2(\Omega)}+\|\nabla\cdot\|_{L^2(\Omega;\mathbb{R}^d)})$. Then, using the discrete Gronwall inequality by a similar way as used for (38), we obtain the estimate for any sufficiently small $\tau>0$:

$$\|\,\overline{c}_{\varepsilon\delta\tau}\|_{L^2(I;H^1(\Omega))}\le C\,. \tag{44}$$

Let us notice that we need the integrability of $m^k_{\varepsilon\delta\tau}\,\nabla\mu^k_{\varepsilon\delta\tau}$ for the legitimacy of the weak formulation, i.e. the integrability of $m^k_{\varepsilon\delta\tau}\varphi''_{cc}(J^k_{\varepsilon\delta\tau},\chi^k_{\varepsilon\delta\tau},c^k_{\varepsilon\delta\tau})\nabla c^k_{\varepsilon\delta\tau}$ and $m^k_{\varepsilon\delta\tau}\varphi''_{Jc}(J^k_{\varepsilon\delta\tau},\chi^k_{\varepsilon\delta\tau},c^k_{\varepsilon\delta\tau})\nabla J^k_{\varepsilon\delta\tau}$, which is indeed guaranteed by the assumed growth conditions in (24c).

Step 4: Convergence for $\tau\to 0$. By the Banach selection principle, we obtain a subsequence converging weakly* with respect to the topologies indicated in (33), (41), and (44) to some limit $(\varrho_{\varepsilon\delta},\boldsymbol{p}_{\varepsilon\delta},\boldsymbol{v}_{\varepsilon\delta},J_{\varepsilon\delta},\chi_{\varepsilon\delta},c_{\varepsilon\delta})$. For the limit passage in (22a-c) we refer to [31].

Due to (44) and an information about $\frac{\partial}{\partial t}\,\overline{c}_{\varepsilon\delta\tau}$, by the (generalized) Aubin-Lions theorem and by interpolation with the $L^\infty(I;L^2(\Omega))$-estimate we already obtained, we have

$$\overline{c}_{\varepsilon\delta\tau}\to c_{\varepsilon\delta}\quad\text{strongly in }\ L^{10/3-a}(I\times\Omega)\ \text{ for any }\ 0<a\le 7/3\,. \tag{45}$$

The weak formulation of the equation in (26e) reads as

$$\begin{aligned}\int_0^T\!\!\int_\Omega \overline{m}_{\varepsilon\delta\tau}\nabla\,\overline{\mu}_{\varepsilon\delta\tau}\cdot\nabla\tilde{c}-\,\overline{c}_{\varepsilon\delta\tau}\,\frac{\partial\tilde{c}}{\partial t}+\,\overline{c}_{\varepsilon\delta\tau}\overline{\boldsymbol{v}}_{\varepsilon\delta\tau}\cdot\nabla\tilde{c}\,\mathrm{d}\boldsymbol{x}\mathrm{d}t&\\ =\int_\Omega c_0\cdot\tilde{c}(0)\,\mathrm{d}\boldsymbol{x}+\int_0^T\!\!\int_\Omega f(\overline{\chi}_{\varepsilon\delta\tau},\,\overline{c}_{\varepsilon\delta\tau})\,\varphi'_c(\overline{J}_{\varepsilon\delta\tau},\overline{\chi}_{\varepsilon\delta\tau},\,\overline{c}_{\varepsilon\delta\tau})\,\tilde{c}\,\mathrm{d}\boldsymbol{x}\mathrm{d}t&\end{aligned} \tag{46}$$

with $\overline{m}_{\varepsilon\delta\tau}=m(\overline{J}_{\varepsilon\delta\tau},\overline{\chi}_{\varepsilon\delta\tau},\,\overline{c}_{\varepsilon\delta\tau})$ to be fulfilled for all smooth $\tilde{c}$ with $\tilde{c}|_{t=T}=0$. Actually, since $\overline{c}_{\varepsilon\delta\tau}>0$ a.e., we have

$$\overline{m}_{\varepsilon\delta\tau}\nabla\,\overline{\mu}_{\varepsilon\delta\tau}=\overline{m}_{\varepsilon\delta\tau}\varphi''_{Jc}(\overline{J}_{\varepsilon\delta\tau},\overline{\chi}_{\varepsilon\delta\tau},\,\overline{c}_{\varepsilon\delta\tau})\nabla\overline{J}_{\varepsilon\delta\tau}\,+\overline{m}_{\varepsilon\delta\tau}\varphi''_{cc}(\overline{J}_{\varepsilon\delta\tau},\overline{\chi}_{\varepsilon\delta\tau},\,\overline{c}_{\varepsilon\delta\tau})\nabla\,\overline{c}_{\varepsilon\delta\tau}\,, \tag{47}$$

and we can eliminate $\overline{\mu}_{\varepsilon\delta\tau}$ from the weak formulation and thus avoid a problem with the expected singularity of $\varphi'_c(J,\cdot)$ at $c=0$ and the limit passage in the variational inequality behind the inclusion $\overline{\mu}_{\varepsilon\delta\tau}\in\varphi'_c(\overline{J}_{\varepsilon\delta\tau},\,\overline{c}_{\varepsilon\delta\tau})$; cf. also [37]. For the limit passage in (46), we need

$$\overline{m}_{\varepsilon\delta\tau}=m(\overline{J}_{\varepsilon\delta\tau},\overline{\chi}_{\varepsilon\delta\tau},\,\overline{c}_{\varepsilon\delta\tau})\to m(J_{\varepsilon\delta},\chi_{\varepsilon\delta},c_{\varepsilon\delta})=:m_{\varepsilon\delta}\quad\text{strongly in }\ L^1(I\times\Omega)\,, \tag{48}$$

which is due to the assumed continuity and growth of m, cf. (24e), and further we need

$$\sqrt{\overline{m}_{\varepsilon\delta\tau}}\nabla\,\overline{\mu}_{\varepsilon\delta\tau}\to\sqrt{m_{\varepsilon\delta}}\nabla\mu_{\varepsilon\delta}\quad\text{weakly in }\ L^2(I\times\Omega;\mathbb{R}^d)\,, \tag{49}$$

which is at our disposal due to the estimate (33d). Thus, for any $\tilde{c}$ smooth, we have

$$\begin{aligned}\int_0^T\!\!\int_\Omega \overline{m}_{\varepsilon\delta\tau}\nabla\,\overline{\mu}_{\varepsilon\delta\tau}\cdot\nabla\tilde{c}\,\mathrm{d}\boldsymbol{x}\mathrm{d}t&=\int_0^T\!\!\int_\Omega\ \underbrace{\sqrt{\overline{m}_{\varepsilon\delta\tau}}\nabla\,\overline{\mu}_{\varepsilon\delta\tau}}_{\substack{\text{converges weakly}\\ \text{by (49)}}}\ \cdot\ \underbrace{\Big(\sqrt{\overline{m}_{\varepsilon\delta\tau}}\nabla\tilde{c}\Big)}_{\substack{\text{converges strongly}\\ \text{by (48)}}}\ \mathrm{d}\boldsymbol{x}\mathrm{d}t\\ &\to\int_0^T\!\!\int_\Omega m_{\varepsilon\delta}\nabla\mu_{\varepsilon\delta}\cdot\nabla\tilde{c}\,\mathrm{d}\boldsymbol{x}\mathrm{d}t\,.\end{aligned} \tag{50}$$

Notably, it does not seem easily possible to pass to the limit directly in (47). Since, due to (41) and (44), we have $\nabla \overline{J}_{\varepsilon\delta\tau} \to \nabla J_{\varepsilon\delta}$ weakly* in $L^\infty(I;L^r(\Omega;\mathbb{R}^d))$ and $\nabla \overline{c}_{\varepsilon\delta\tau} \to \nabla c_{\varepsilon\delta}$ weakly in $L^2(I\times\Omega;\mathbb{R}^d)$. Then, due to the continuity and the growth assumptions (24c), we have the strong convergence

$$\begin{aligned}
&\overline{m}_{\varepsilon\delta\tau}\varphi''_{Jc}(\overline{J}_{\varepsilon\delta\tau},\overline{\chi}_{\varepsilon\delta\tau},\overline{c}_{\varepsilon\delta\tau}) \to m_{\varepsilon\delta}\varphi''_{Jc}(J_{\varepsilon\delta},\chi_{\varepsilon\delta},c_{\varepsilon\delta}) \qquad \text{in } L^{10/3-a}(I\times\Omega) \text{ and}\\
&\overline{m}_{\varepsilon\delta\tau}\varphi''_{cc}(\overline{J}_{\varepsilon\delta\tau},\overline{\chi}_{\varepsilon\delta\tau},\overline{c}_{\varepsilon\delta\tau}) \to m_{\varepsilon\delta}\varphi''_{cc}(J_{\varepsilon\delta},\chi_{\varepsilon\delta},c_{\varepsilon\delta}) \qquad \text{in } L^{10/9}(I\times\Omega)
\end{aligned}$$

with $a>0$ as in (45). Thus, interestingly, $m(\overline{J}_{\varepsilon\delta\tau},\overline{c}_{\varepsilon\delta\tau})\nabla\overline{\mu}_{\varepsilon\delta\tau}$ is "optically" even not integrable when seen directly from (47), but anyhow (50) serves well. The limit passage in the last term in (46) is simple due to the (even strong) convergence $f(\overline{\chi}_{\varepsilon\delta\tau},\overline{c}_{\varepsilon\delta\tau})\varphi'_c(\overline{J}_{\varepsilon\delta\tau},\overline{\chi}_{\varepsilon\delta\tau},\overline{c}_{\varepsilon\delta\tau}) \to f(\chi_{\varepsilon\delta},c_{\varepsilon\delta})\varphi'_c(J_{\varepsilon\delta},\chi_{\varepsilon\delta},c_{\varepsilon\delta})$; here the continuity and growth assumption (24f) was used. Altogether, we obtain a weak solution of the system (19) with the corresponding initial and boundary conditions.

Step 5: Further a-priori estimates and convergence for $\delta\to0$ and $\varepsilon\to0$. The rest of the proof just expands [31, Sect.3] by the limit passage in (19), so that we will only sketch the arguments.

The mechanical part is even simplified compared to [31] because φ depends on the Jacobian J instead of the full deformation gradient as considered in [31] and is convex. Another simplification is the (hyper)visco-elastic rheology of the mere Stokes' type instead of the Jeffreys one as considered in [31]. Eventually, the mollification of the stored energy in [31] has here been avoided because the singularity at $J=0$ is here avoided due to assumption of a stronger growth (24b) which allows for usage of the Healey-Krömer argumentation [17].

In particular, we can test the continuity equation (19a) by $\mathrm{div}(|\nabla\varrho_{\varepsilon\delta}|^{r-2}\nabla\varrho_{\varepsilon\delta})$ obtaining the $L^\infty(I;W^{1,r}(\Omega))$-estimate of $\varrho_{\varepsilon\delta}$. Then we can eliminate the cut-off $\mathcal{I}$ due to the previous choice of $\rho_{\max}$ in Step 1. Also the J-equation (19c) can be tested by $\Delta J_{\varepsilon\delta}$ to obtain the $L^\infty(I;H^1(\Omega))$-estimate of $J_{\varepsilon\delta}$. As (26c) does not contain any regularizing term, the limit passage with $\delta\to0$ is simpler comparing to [31]. After passing with $\delta\to0$ to the limit, we can also estimate ϱ_ε from below and then, from the bound of the kinetic energy in the form $\frac12\varrho_\varepsilon|\boldsymbol{v}_\varepsilon|^2$, obtain the $L^\infty(I;L^2(\Omega;\mathbb{R}^d))$-bound of $\boldsymbol{v}_\varepsilon$. This eventually allow for passage to the limit with $\varepsilon\to0$.

Since (19e) does not involve any regularizing (ε,δ)-terms, the limit passages in this additional equation just copies the arguments from Step 4. □

Example 3.3 (*Biot-type stored energy*)**.** The assumptions (24a–c) are not straightforward to be compatible with reasonable applications. For the Biot modulus $B>0$ and the Biot coefficient b, an example can be

$$\begin{aligned}
&\varphi_{\mathsf{R}}(J,\chi,c)=\chi^2\kappa_{\mathsf{R}}(J)+J\varphi_{\mathrm{poro}}(J,\chi,c) \quad\text{and}\quad m(J,\chi,c)=m_0(J,\chi)c\\
&\text{where}\qquad \varphi_{\mathrm{poro}}(J,\chi,c)=\chi^2\frac{B}{2}(b(J-J_{\mathrm{ref}})-c)^2+\epsilon c\left(\ln\frac{c}{c_{\mathrm{ref}}}-1\right),
\end{aligned}\tag{51}$$

with some $\epsilon>0$ and with the "referential" $\kappa_{\mathsf{R}}\ge0$ having the sufficiently fast blowup at $J=0$, namely $\liminf_{J\to0+}\kappa_{\mathsf{R}}(J)/J^{s-1}>0$ with s from (24b) so that the "actual" energy term $\kappa(J)=\kappa_{\mathsf{R}}(J)/J$ satisfies (24b) and is expected to be convex. Recalling $\varphi(J,\chi,c)=\varphi_{\mathsf{R}}(J,\chi,c)/J$ the pressure and the chemical potential are respectively

$$\begin{aligned}
p(\boldsymbol{q}) &\overset{(1b)}{=} -[\varphi_{\mathsf{R}}]'_J(\chi,J,c)+\frac{c}{J}[\varphi_{\mathsf{R}}]'_c(\chi,J,c)\\
&= -\chi^2\kappa'_{\mathsf{R}}(J)-\Big(\varphi_{\mathrm{poro}}(\chi,J,c)+J[\varphi_{\mathrm{poro}}]'_J(\chi,J,c)-c[\varphi_{\mathrm{poro}}]'_c(\chi,J,c)\Big), \qquad (52a)\\
\mu(\boldsymbol{q}) &\overset{(1e)}{=} [\varphi_{\mathrm{poro}}]'_c+RV \quad\text{with } V(\boldsymbol{x})=-\boldsymbol{g}\cdot\boldsymbol{x}, \qquad \text{where } \boldsymbol{g}=(0,-9.8\,\mathrm{m\,s^{-2}}). \qquad (52b)
\end{aligned}$$

Furthermore, we have

$$m(J,\chi,c)\varphi''_{cc}(J,\chi,c)=Bm_0(J,\chi)c+\epsilon m_0(J,\chi) \quad\text{and}\quad m(J,\chi,c)\varphi''_{Jc}(J,c)=-bm_0(J,\chi)Bc \tag{53}$$

and (24c) is satisfied provided $m_0(\cdot)$ is continuous and positive. Note that m satisfies also (24g).

Example 3.4 (*Convexity of the stored energy)***.** The convexity of φ assumed in (24a) is not easy to maintain in a general dependence on χ. In the scalar-valued situation when the composition field can be exploited as an air-mantle indicator to facilitate the so-called *sticky-air strategy*, i.e., the introduction of a passive ambient air phase, one can consider $\varphi(J,\chi,c)=\chi^2\phi(J,c)$. In accord to the above examples, we can assume ϕ convex. The desired convexity then depends on the positive semidefiniteness of the Hessian, which essentially reduces, through the Sylvester's criterion, to the non-negativity of its determinant, *i.e.*, abbreviating $q=(J,c)$ and writing $\varphi(q,\chi)=\chi^2\phi(q)$,

$$\det\varphi''(q,\chi)=\det\begin{pmatrix}\chi^2\phi''(q) & , & 2\chi\phi'(q)\\ \chi\phi'(q) & , & 2\phi(q)\end{pmatrix}=2\chi^2\big(\underbrace{\phi(q)\phi''(q)-2\phi'(q)^2}_{\text{to be non-negative}}\big)\,. \tag{54}$$

Of course, since q has two components, the involved derivatives are vector- or matrix-valued. The desired non-negativity of (54) is rather delicate, but counting an active range of J's and c's, the energy ϕ can be considered uniformly convex; note that the affine flat part of κ_{R} in Figure 1-left below become strictly convex in $\kappa=\kappa_{\mathsf{R}}/J$. Moreover, one can consider a bounded slope ϕ' on the active range of parameters (in particular when c stays away from zero to avoid the singularity of the last terms in (52b). Importantly, ϕ acts in the problem (1) only through its derivatives, so a sufficiently large constant can be added to ϕ to make the positive term $\phi(q)\phi''(q)$ dominating the non-positive term $2\phi'(q)^2$.

4 Application to phase transition and (de)hydration of rocks

This section presents a numerical implementation of the above model on the Earth's mantle dynamics, which is only one of many possible applications. Among many phenomena studied in this area, we focus on a heavier hydrated part (typically arising from the uppermost crust) which descents into viscous asthenosphere and sometimes even deeper into the lower mantle. As such sort of modelling counts with the timescale millions of years and relatively slow movements, the inertial effects are negligible and one can confine to a *quasistatic* variant of (1) as in Remark 2.2.

Such descending slabs are usually modelled as incompressible while the exo- or endothermal phase transitions are made by exploiting temperature dependence, cf. *e.g.* [1, 5, 7, 9, 36], even though the thermodynamical consistency (in particular energy conservation) is often not fully pursued, not mentioning adiabatic effects which are naturally suppressed in incompressible models. Here, we show that even an isothermal variant can model such phase transition if the compressibility is taken into account in an appropriate way. Occasionally, compressible models as [12, 20, 33, 34] or "semi-compressible" [3] are reported in literature. Of course, involving temperature into the model would presumably refine the model towards the full state-equation description, although this is out of the scope of this paper.

4.1 Modelling of the volumetric phase transitions in the Earth's mantle

There are several phase transitions in the Earth's mantle, specifically at the levels 410 km, 520 km, and 660 km. We model here only in the last one, which is the main discontinuity distinguishing the so-called mantle transition zone (where a lot of water chemically bonded in minerals is deposited) as a bottom part of the upper mantle and the lover mantle which goes from 660 km to 2 900 km deep.

Realistic data for this *660 km phase transition* under the pressure p_{T}=24 GPa with the jump of the mass density $\sim$8.5%: (this *density contrast* is sometimes specified 342 kg m^{-3} in literature [9]) while the rock above (in the lithosphere and asthenosphere forming the upper mantle) increases its density by $\sim 10\%$ from ϱ_0=3600 kg m^{-3} on the Earth uppermost mantle. A simplified, for $J>J_{\mathsf{CMB}}$ piecewise quadratic C^1-ansatz for the volumetric

part of the referential stored energy is

$$\kappa_{\mathsf{R}}(J)=p_{\mathsf{T}}\Big(-J+\big(J_{\mathsf{CMB}}/J-1\big)_+^2\Big)+\begin{cases}\frac{1}{2}K_1(J-J_1)^2 & 0<J<J_1\\ 0 & J_1\le J\le J_2\\ \frac{1}{2}K_2(J-J_2)^2 & J>J_2\end{cases} \tag{55}$$

with parameters from Table 2. The corresponding pressure is

$$p=-\kappa_{\mathsf{R}}'(J)=p_{\mathsf{T}}+\begin{cases}K_1(J_1-J)+2p_{\mathsf{T}}\big(J_{\mathsf{CMB}}/J-1\big)J_{\mathsf{CMB}}/J^2\big) & \text{for } 0<J<J_{\mathsf{CMB}}\,,\\ K_1(J_1-J) & \text{for } J_{\mathsf{CMB}}\le J<J_1\,,\\ 0 & \text{for } J_1\le J\le J_2\,,\\ K_2(J_2-J) & \text{for } J>J_2\,.\end{cases} \tag{56}$$

The specific values for J_i's and K_i's are taken at $J=J_2$, the pressure attains p_{T} and the mass density $\varrho=\varrho_0/J=\varrho_0/(1-p/K)$ at $p=p_{\mathsf{T}}$ is 3600/0.9 = 4000 kg m^{-3}; thus K_2=240 GPa although the conventional values of the first Lamé modulus K are about 10–30 GPa. During the phase transition, the mass density $\varrho=\varrho_0/J$ jumps to 3600/0.83 $\doteq$ 4 340 kg m^{-3}. On the core-mantle boundary at the depth 2900 km, the pressure is about 130 GPa and the density is $\sim$ 5300 kg m^{-3}, which corresponds to $J_{\mathsf{CMB}}\sim 0.68$; cf. the standard Preliminary Reference Earth Model (PREM) [11]. This leads to the value $K_1\sim$ 620 GPa for (55). For $J<J_{\mathsf{CMB}}$, the hydrated rock model is not relevant since rocks in mantle never can penetrate into the metallic core, which is why we can formally add some contribution which has an expected blow up for $J\to 0+$; in fact, the referential-energy blow-up in (55) causes the asymptotics of the actual stored energy $\sim 1/J^2$ for $J\to 0+$, while the blow-up condition (24b) would need a higher growth. This is schematically illustrated in Figure 1; actually (55) is depicted shifted by a constant which would give $\kappa_{\mathsf{R}}(1)=0$ and it should be realized that such a constant is irrelevant for the time-continuous problem and for the time-discrete problem (22), too, but may influence convexity of the actual κ needed for the estimation (30) and thus the resulted a-priori estimates.

Let us remark that the actual density profile depending on the pressure (which is approximately proportional to the depth) should be rather piecewise concave instead of convex as on Figure 1-right, so the piecewise quadratic ansatz used in (55) for $J>J_{\mathsf{CMB}}$ should be more complicated. Noteworthy, the convexity of the actual energy $\kappa(J)=\kappa_{\mathsf{R}}(J)/J$ exploited in (29) is inherited from the convexity of κ_{R}; here we realize also the fact that κ is non-negative (if calibrated so that $\kappa_{\mathsf{R}}(1)=0$) and non-increasing so that $\kappa''(J)=\kappa_{\mathsf{R}}''(J)/J-2\kappa_{\mathsf{R}}'(J)/J^2+2\kappa_{\mathsf{R}}(J)/J^3\ge 0$.

4.2 Discretization in space and time

The time discretization of the model proposed and analysed in Section 3 has been accompanied by a finite-element space discretization and several shortcuts have been adopted for its implementation in FEniCS [21]. First, the higher-order viscosity which facilitated the analysis in Section 3 was neglected, i.e. $\nu=0$. As previously mentioned, any inertia is neglected for modelling the million-year time scale so the only quasistatic variant was implemented.

We solve a fully Eulerian compressible fluid model on a fixed domain Ω, where the basic air-mantle heterogeneity is tracked using an indicator function $\chi:[0,T]\times\Omega\to\mathbb{R}$. Therefore, the set of unknowns is $\boldsymbol{q}=(\varrho,c,\boldsymbol{v},J,\chi):[0,T]\times\Omega\to\mathbb{R}\times\mathbb{R}\times\mathbb{R}^d\times\mathbb{R}\times\mathbb{R}$ with the meaning as in Table 1. In the following examples, $\chi\approx 1$ indicates the rock phase while $\chi\approx 0$ indicates the complementary air phase. This representation of the air phase is used because, under gravitational forces, the initially uncompressed fluidic rock will compress into a stress-free state, for which the air–rock interface is *a priori* unknown.

We discretize in FEniCS using scalar P_1 finite elements for ϱ,c,J,χ and using vectorial P_1 finite elements for $\boldsymbol{v}$. The solution at time t^k is denoted by $\boldsymbol{q}(t^k)=\boldsymbol{q}^k=(\varrho^k,c^k,\boldsymbol{v}^k,J^k,\chi^k)\in Q_h$ with initial data $\boldsymbol{q}^0=(\varrho_0,c_0,\boldsymbol{v}_0,J_0,\chi_0)$ at time $t^0=0$. We discretize the problem by formulating a nonlinear residual using

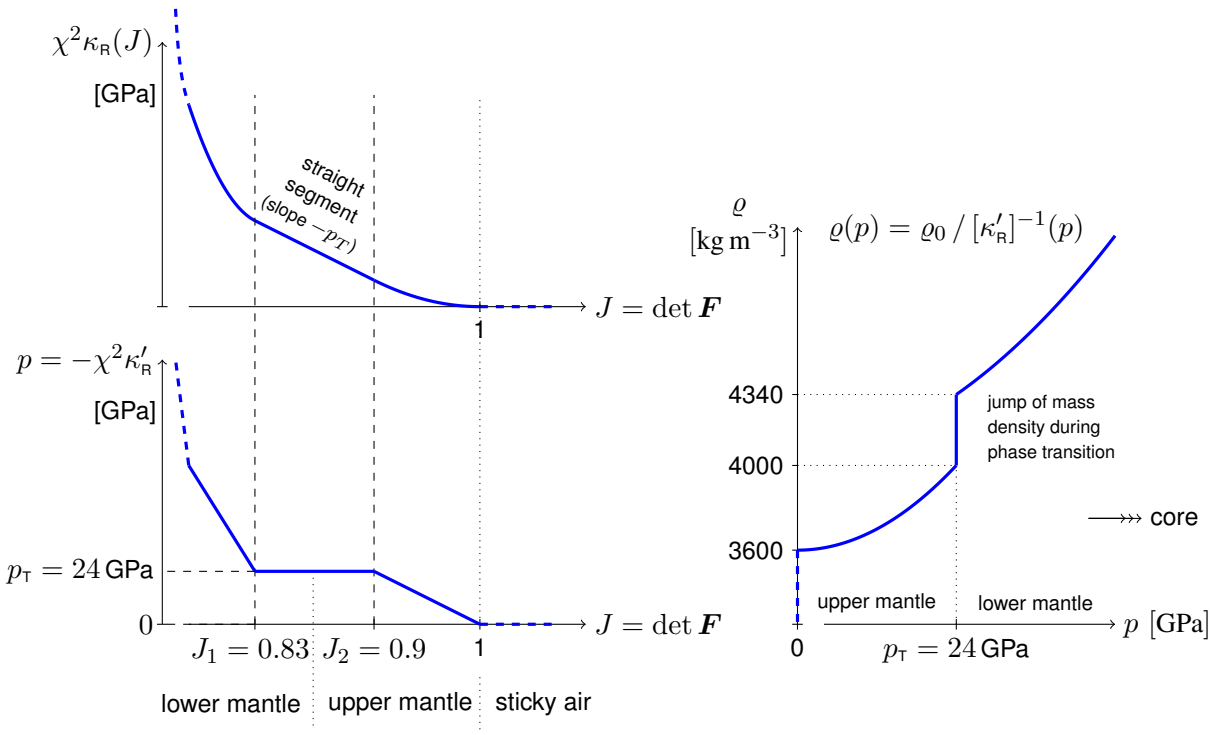

Figure 1: *A schematic illustration of one phase transition (rock compaction) when pressure reaches a critical value* p_T *calibrated to a basic scenario of the phase transition at* $p_T = 24\,\mathrm{GPa}$ *with the density contrast* $340\,\mathrm{kg/m^3}$ *which is realized at the depth* $660\,\mathrm{km}$ *below the Earth's surface.*

test functions $\boldsymbol{w} = (w_\varrho, w_c, \boldsymbol{w_v}, w_J, w_\chi) \in Q_h$, where at time $t = t^k$

$$
\begin{aligned}
\langle \mathscr{R}_k(\boldsymbol{q}^k), \boldsymbol{w}\rangle = \int_\Omega\ & 2\eta_{\mathrm{eff}}(\boldsymbol{q}^{k-1})\mathbb{D}(\boldsymbol{v}^k) : \mathbb{D}(\boldsymbol{w_v}) - p(\boldsymbol{q}^k)\nabla\cdot\boldsymbol{w_v} \\
&\quad - \boldsymbol{f}_{\mathrm{grav}}(\boldsymbol{q}^k)\cdot\boldsymbol{w_v} + \kappa_{\mathrm{eff}}(\boldsymbol{q}^{k-1})(\nabla\cdot\boldsymbol{v}^k)(\nabla\cdot\boldsymbol{w_v})\,\mathrm{d}\boldsymbol{x} \\
&+ \int_\Omega \frac{c^k - c^{k-1}}{\tau^k} w_c - \left[\theta c^k \boldsymbol{v}^k + (1-\theta)c^{k-1}\boldsymbol{v}^{k-1} - m(\boldsymbol{q}^{k-1})\nabla\mu(\boldsymbol{q}^k)\right]\cdot\nabla w_c\,\mathrm{d}\boldsymbol{x} \\
&+ \int_\Omega \frac{\varrho^k - \varrho^{k-1}}{\tau^k} w_\varrho - \left[\theta \varrho^k \boldsymbol{v}^k + (1-\theta)\varrho^{k-1}\boldsymbol{v}^{k-1}\right]\cdot\nabla w_\varrho\,\mathrm{d}\boldsymbol{x} \\
&+ \int_\Omega \frac{J^k - J^{k-1}}{\tau^k} w_J + \left[\theta \boldsymbol{v}^k\cdot\nabla J^k + (1-\theta)\boldsymbol{v}^{k-1}\cdot\nabla J^{k-1}\right] w_J \\
&\quad - \left[\theta J^k \nabla\cdot\boldsymbol{v}^k + (1-\theta)J^{k-1}\nabla\cdot\boldsymbol{v}^{k-1}\right] w_J\,\mathrm{d}\boldsymbol{x} \\
&+ \int_\Omega \frac{\chi^k - \chi^{k-1}}{\tau^k} w_\chi + \left[\theta \boldsymbol{v}^k\cdot\nabla\chi^k + (1-\theta)\boldsymbol{v}^{k-1}\cdot\nabla\chi^{k-1}\right] w_\chi + \\
&\quad \frac{\varepsilon_{\mathrm{reg}}}{\tau^k}\left[\nabla\varrho^k\cdot\nabla w_\varrho + \nabla J^k\cdot\nabla w_J + \nabla\chi^k\cdot\nabla w_\chi\right]\mathrm{d}\boldsymbol{x}
\end{aligned}
$$

In order to avoid excess diffusion for large time-steps and high convection velocities, we can set $\theta = 1/2$. Otherwise, a fully implicit discretization with $\theta = 1$ (except for the effective viscosity) would be more in line with the time discretization in the preceding sections of this paper. We will also use an adaptive time-stepping strategy, where $\tau^k = t^k - t^{k-1}$ can be adapted based on solution or solver requirements, *e.g.*, the number of Newton iterations to solve the nonlinear equation $\mathscr{R}_k(\boldsymbol{q}^k) = 0 \in Q_h^*$. The small parameter $\varepsilon_{\mathrm{reg}}$ regularizes the hyperbolic nature of the continuity equations to facilitate stability of the time-discretization that is being solved via a Newton iteration within the FEniCS framework. The particular scaling of the regularization with τ^k ensures that

the influence of the artificial diffusion diminishes as the adaptive time step τ^k increases during the simulation and the parameter $\varepsilon_{\rm reg}$ is chosen small enough such that the introduced diffusion remains negligible during the initial phase of the simulation, where time steps are small and accurate resolution of steep gradients is critical.

For the stored energy we use the representation from Equation (51) with volume contributions as introduced in Equation (55) and corresponding pressure and chemical potential from Equation (52). The shear viscosity is (60) with $f_{\rm visc}(J) = \exp\big(p_J = (J - J_2)\big)$, where this specific dependence is tuned so that with $p_J = -33$ we observe a realistic contrast of viscosity at the 660 km discontinuity increasing by a factor 10 or more transitioning from the upper to the lower mantle, *e.g.*, see [8, 12], or have a viscosity that is independent from volume via $p_J = 0$. Furthermore, we chose bulk viscosity and mobility to be $\kappa_{\rm eff}(\boldsymbol{q}) := \kappa$ and $m(\boldsymbol{q}) := m_0 c$.

4.3 Stratification due to gravitation and volumetric phase transitions

A certain advantage of the Eulerian approach used here is no need of remeshing of the space discretization even within long time scale simulations but, on the other hand, a disadvantage is the need of a fixed computational domain which is reflected by the boundary condition $\boldsymbol{v}\cdot\boldsymbol{n} = 0$ as used in (13).

In the simulations of the Earth's mantle dynamics which we have in mind in this section, one should cope with a time varying topography of the Earth surface. This is standardly handled by considering also the adjacent atmosphere as light weak-viscosity medium which does not substantially influence the heavy highly viscoelastic mantle. This rather numerical concept is known in computational geophysics as the sticky-air approach [10] while in engineering it is known as a fictitious-domain approach or as an immersed-boundary method. Here we execute this idea by using the composition scalar-valued field χ, relying also on the convexity in Remark 3.4.

In the gravitational field V, the medium stratifies in its steady state and even the phase transition as in Figure 1 leads to forming an interface where the density jumps. Of course, another jump of density is formed on the air-mantle interface. This transient event started from purely artificial initial condition, where for $(x, z) = \boldsymbol{x} \in \Omega$ at initial time $t_0 = 0$ we have

$$\varrho_0(\boldsymbol{x}) = \varrho_{\rm air}(1 - \chi_0(\boldsymbol{x})) + \varrho_{\rm rock}\chi_0(\boldsymbol{x}), \qquad \chi_0(\boldsymbol{x}) = \tfrac{1}{2}\big(1 + \tanh(\tfrac{1}{\varepsilon}(z - h_0))\big), \tag{57}$$

where $\varepsilon = 20\,\mathrm{km}$ is the size of the initial transition layer between rock and air. The computational domain is $\Omega = [0, 1000\,\mathrm{km}] \times [0, 2500\,\mathrm{km}]$, with the initial rock air interface at $h_0 = 2000\,\mathrm{km}$. The initial concentration and volume are spatially uniform $c_0(\boldsymbol{x}) = c_0 = 0.005 \in \mathbb{R}$ and $J_0(\boldsymbol{x}) = 1$. For the flow problem we chose boundary conditions $\boldsymbol{v}(t, \boldsymbol{x}) = \boldsymbol{0}$ for at $z = 0$ and $z = 2500\,\mathrm{km}$ and $\boldsymbol{v}(t, \boldsymbol{x}) \cdot \boldsymbol{n} = 0$ for $x = 0$ and $x = 1000\,\mathrm{km}$ and homogeneous Neumann boundary conditions for the z-component, *i.e.*, sliding walls. The boundary conditions for all other equations are homogeneous natural boundary conditions. The transition to the steady mass density of this model with the parameters from Table 2 is shown in Figure 2 with times t increasing from left to right. While the upper discontinuity of the density from $\varrho \approx 4000\,\mathrm{kg\,m^{-3}}$ almost vanishing mass density $\varrho \approx 0$ in the air phase is generated by the initial data ϱ_0 and the indicator χ, the lower discontinuity is generated by the equation of state encoded in the stored energy density $\kappa_{\rm R}$ of the compressible model. The jump gradually appears about $600\,\mathrm{km}$ below the upper rock-air interface as $t \to \infty$. This figure exemplifies a key feature of this model: Heterogeneities in the composition of the earth can be encoded using indicator functions χ, whereas discontinuities emerge using the equation of state of the stored energy function.

The purely quasistatic visco-elastic simulations from Section 4.3 can govern also a dehydration process in the sense that, although both phenomena are mutually coupled, the former is dominant while the dehydration rather follows, cf. [33] where dehydration is completely decoupled from the mechanical part of the model. Depending on the choice of parameters in Biot's poroelasticity, we obtain slightly different fluid content $c(\boldsymbol{x})$ in the stationary state $t \to \infty$. Note that due to the regularization parameter $\varepsilon_{\rm reg}$, we do not reach the fully stationary state but stop the simulation at a sufficiently large finite time T. In the equation of state (51), we assume that the density ϱ or volume J are primarily determined by $\kappa_{\rm R}(J)$, and that the concentration dependence in $\varphi_{\rm poro}$ more or less follows the given volume J or density ϱ. This leads to a competition between gravity acting on fluid

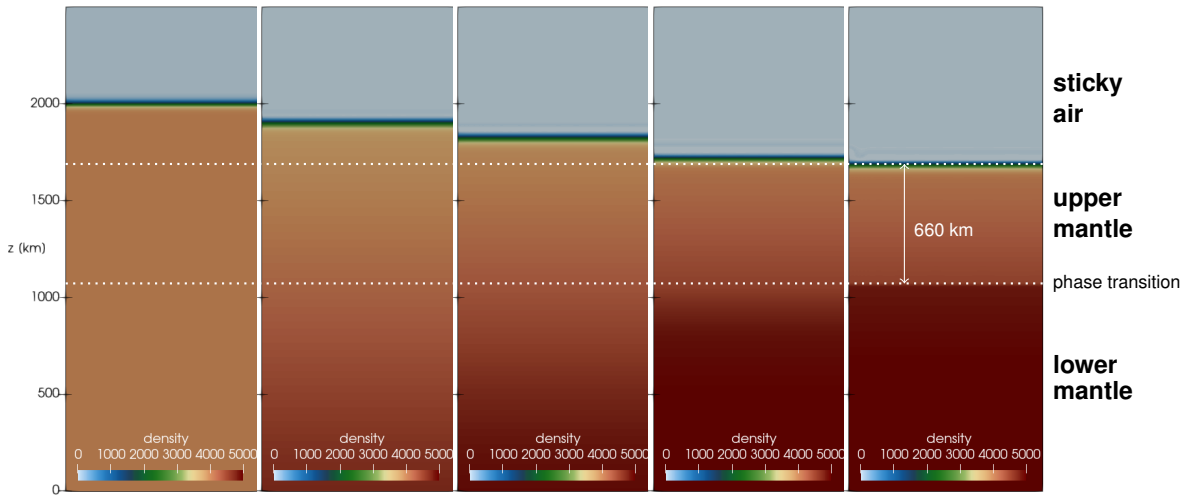

Figure 2: Transient process (mostly compression in the mantle) from left to right of the mass density, started from an artificial initial Earth mantle layer of thickness $2000\,\mathrm{km}$, see Equation (57), evolving to a stratified stationary state. The corresponding final stationary density shows the air/upper-mantle/lower-mantle layered structure with a sharp density jump about $660\,\mathrm{km}$ below the air/mantle interface determined mainly by the elastic rock property from Figure 1.

quantity	value	unit	quantity	value	unit
c_{ref} in (51)	0.02	1	K_2	240	GPa
ϱ_{rock} in (57)	4000	$\mathrm{kg\,m^{-3}}$	p_{T}	$K_2(1-J_2)$	GPa
ϱ_{air} in (57)	40	$\mathrm{kg\,m^{-3}}$	Bb^2	$0.005\,K_1$ or $0.05\,K_1$	GPa
μ_{dif} in (60)	10^{20}	$\mathrm{Pa\,s}$	b	0.1	1
μ_{Sks} in (60)	10^{17}	$\mathrm{Pa\,s}$	J_1	0.83	1
μ_{dsl} in (60)	$3.4\cdot 10^{12}$	$\mathrm{Pa\,s}^{1/n}$	J_2	0.9	1
n in (60)	3.5	1	J_{CMB}	0.68	1
K_1	620	GPa	J_{ref}	$\frac{1}{2}(J_1+J_2)$	1
$\lvert\nabla V\rvert = \lvert\boldsymbol{g}\rvert$	9.8	$\mathrm{m\,s^{-2}}$			

Table 2: List of model parameters used in the simulation.

content (downward force), fluid motion towards regions of lower pore pressure (usually an upward force), and the redistribution of fluid content due to the (weak regularizing) logarithmic dependence in the equation of state.

Therefore, in Figure 3, we show in the left panel the stationary concentration profile when the gravitational force on the fluid content is weaker than the pore pressure gradient, compared to the opposite situation—shown in the right panel, where gravity dominates over the pore pressure. In the former case, the fluid content is higher in the upper mantle, where pore pressure is lower due to the larger volume $J > J_2$. In the latter case, the fluid content is higher in the lower mantle, right towards the bottom. It is very likely that introducing temperature dependence would result in more complex parameter regimes for steady states.

4.4 Simulation of (de)hydration in descending slabs or ascending plumes

We consider a local perturbation of the stationary states from Section 4.3 by using initial data

$$c_0(\boldsymbol{x}) = c(\boldsymbol{x}) + \frac{\delta c}{2}\Big(1+\tanh\big(\tfrac{1}{\delta r^2}(r^2-|\boldsymbol{x}-\boldsymbol{x}_0|^2)\big)\Big), \tag{58}$$

where $\delta c = 0.05$ and $\delta r = 71\,\mathrm{km}$. In the following we investigate two scenarios:

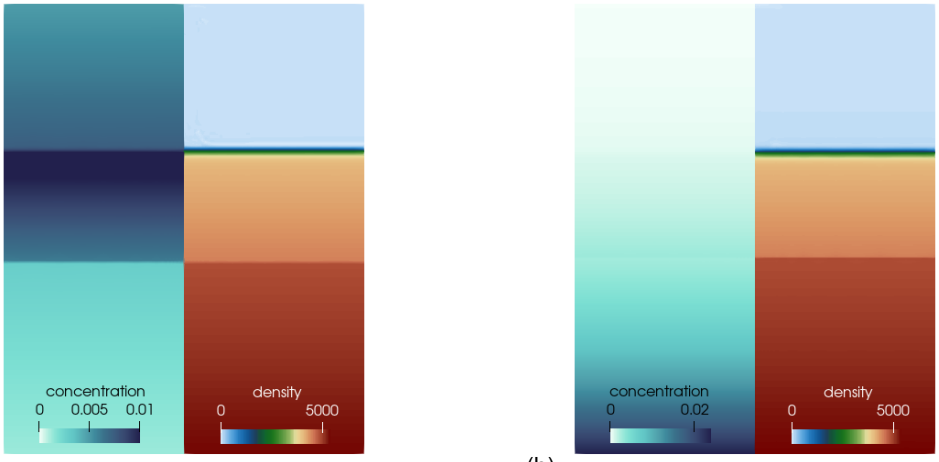

(a) (b)

Figure 3: Various stationary fluid content distribution and the corresponding mass density in the Earth layered mantle: left (a) with Biot's pore pressure dominating over fluid gravity and right (b) with fluid gravity dominating over pore pressure.

- **gravity dominates** over pore pressure: $R = 1$, $Bb^2 = 0.005K_1$ leading to a descending slab and fluid is concentrated at $\boldsymbol{x}_0$ in the upper mantle;
- **pore pressure dominates** over gravity: $R = 0.2$, $Bb^2 = 0.05K_1$ leading to an ascending plume and fluid is concentrated at $\boldsymbol{x}_0$ in the lower mantle.

Additionally, the effective viscosity modulus in the mantle typically ranges in $10^{20} - 10^{23}$ Pa·s and is shear-rate dependent, specifically it is dominated by dislocation creep resulting in a non-Newtonian (plastic-type) dislocation viscosity. This leads to a shear-thinning material behaviour and causes lubrication effects in the vicinity of a descending slab. Dislocation creep is also strongly temperature and volume (J) dependent and thereby may lead to stagnation effects at the interface between upper and lower mantle due to the viscosity contrast across the 660 km phase transition, cf. *e.g.*, [8, 28]. While the temperature dependence is not considered here, the compressible nature of the model allows us to distinguish between the viscosities associated with the volumetric flow $\mu_{\rm vol}$ and the shear (deviatoric) flow $\mu_{\rm dev}$ by expressing the viscosity tensor $\mathbb{D}$ as

$$\boldsymbol{D} = \mathbb{D}(J, \chi, c, \boldsymbol{\varepsilon}(\boldsymbol{v}))\,\boldsymbol{\varepsilon}(\boldsymbol{v}) = \mu_{\rm vol}\,{\rm tr}\,\boldsymbol{\varepsilon}(\boldsymbol{v})\,\mathbb{I} + \mu_{\rm dev}\,{\rm dev}\,\boldsymbol{\varepsilon}(\boldsymbol{v}), \tag{59}$$

where ${\rm dev}\,\boldsymbol{\varepsilon} := \boldsymbol{\varepsilon} - \frac{1}{d}({\rm tr}\,\boldsymbol{\varepsilon})\,\mathbb{I}$ for $\boldsymbol{\varepsilon} \in \mathbb{R}^{d\times d}$. Here we consider $\mu_{\rm vol}$ constant, while the shear viscosity $\mu_{\rm dev}$ is considered of the serial-like combination of the so-called dislocation viscosity $\mu_{\rm dsl} = \mu_{\rm dsl}(|{\rm dev}\boldsymbol{\varepsilon}(\boldsymbol{v})|)$ and diffusion viscosities $\mu_{\rm dif}$ (phenomenologically using the harmonic mean [30]) together with the Stokes-type viscosity $\mu_{\rm Sks}$ in parallel to avoid the degeneracy of the effective shear viscosity. Moreover, a J-dependent factor is considered to implement the viscosity jump at the volumetric phase transition. Altogether, the effective shear viscosity is considered as

$$\mu_{\rm dev} = \mu_{\rm dev}(J, |{\rm dev}\boldsymbol{\varepsilon}(\boldsymbol{v})|) = \mu_{\rm Sks} + \frac{f_{\rm visc}(J)}{1/\mu_{\rm dif} + |{\rm dev}\boldsymbol{\varepsilon}(\boldsymbol{v})|^{1-1/n}/\mu_{\rm dsl}}\,, \tag{60}$$

with the exponent $n = 3.5$, which is the most common choice of the power-law dislocation viscosity. Such viscosity laws with state-dependent viscosity $f_{\rm visc}(J) \sim {\rm e}^{(E+p_J J)/k_B T}$ can be found in literature, cf. *e.g.* [5, 7, 8, 9, 13, 28, 36]. Such a shear-weakening viscosity in a non-Newtonian fluid model leads to localized high shear rates, which correspond to regions of reduced effective viscosity in slab or plume interfaces, thereby facilitating the movement of these structures through the Earth's mantle. The J-dependence in (60) encoded in $f_{\rm visc}$ causes the viscosity contrast within the phase transition (i.e. between the lower and the upper mantle), which in particular may lead to stagnation of descending slabs on the bottom of the upper mantle. In the following we use a constant $p_J \le 0$ so that compressed lower mantle has a higher shear viscosity.

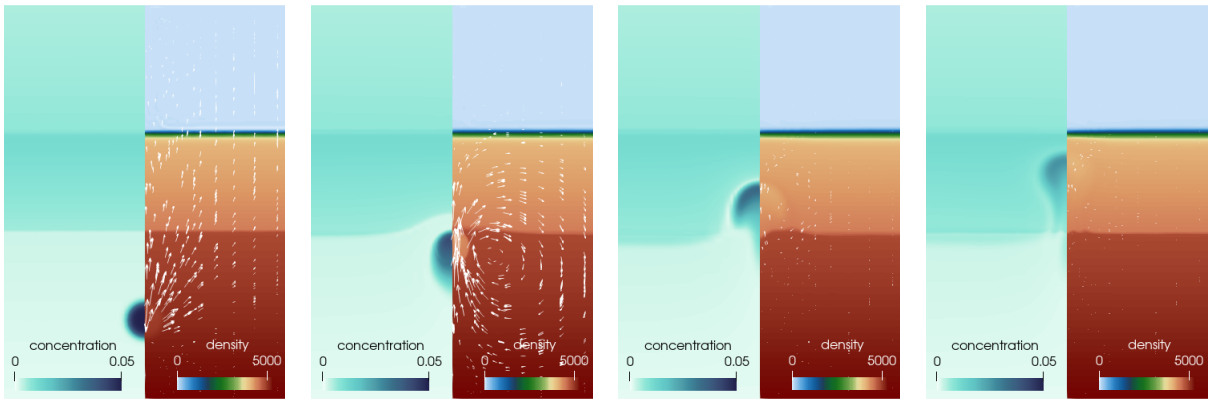

Figure 4: A drop-like plume ascending from the lower mantle to the upper mantle, depicted at selected four times instants $t = \{0, 226, 313, 405\} \cdot 10^3$ y from left to right with the pore pressure dominating (without volume dependence of dislocation viscosity $p_J = 0$). The left part of each panel shows the fluid content c, whereas the right part shows the mass density together with the velocity field.

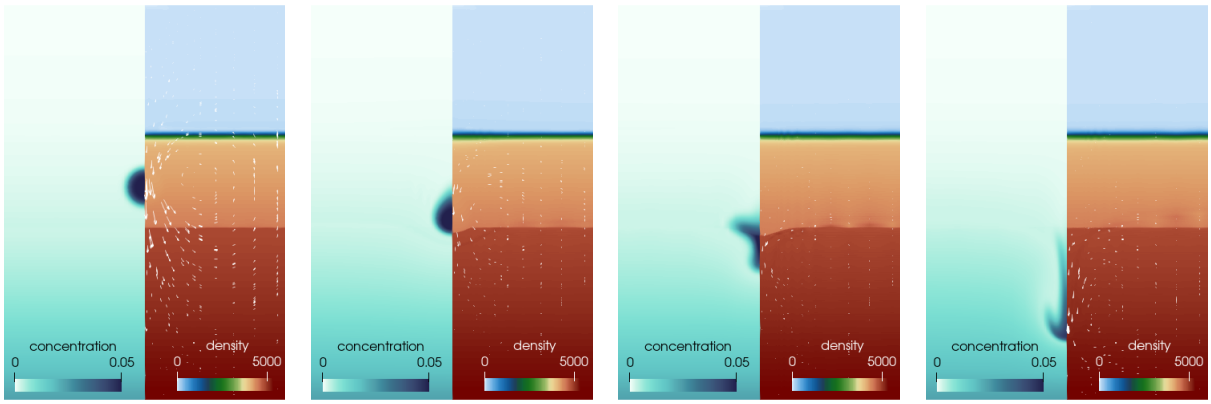

Figure 5: Descending drop-like slab at times $t = \{0, 93, 915, 1305\} \cdot 10^3$ y with gravity dominating (without volume dependence of dislocation viscosity $p_J = 0$), undergoing the transition in between the upper and the lower mantle without substantial dehydration.

A typical simulation in the regime where pore pressure dominates and causes a drop-like plume to ascend is shown in Figure 4. In each panel of this time series, the left part displays the fluid content, whereas the right part shows the mass density. The volumetric phase transition (light to dark brown) clearly visible in the mass density at a depth of 660 km beneath the rock–air interface (light brown to light blue). Despite the downward buoyancy force generated by the fluid content, the drop rises due to pore pressure gradients modelled by the compressible Stokes model. The simulation captures coherent plume ascent accompanied by localized transient vortex structures that are modelled by the shear-thinning rheology. The coupling between fluid content and density via the equation of state induces a slight topographic deformation of the phase transition in the mass density field. This effect is reproduced without invoking volume-dependent viscosity, underscoring the capability of the model to simulate large-scale poro-visco-elastic flow.

Similarly, in Figure 5 we show a descending slab in the regime where gravitational forces dominate, evolving over more than a million years. The drop initially approaches the phase transition, indents the interface with some resistance due to the additional energetic barrier from elevated pore pressure, and then continues its descent into the lower mantle. The localization of strain rate due to dislocation viscosity is clearly visible, most prominently in the rightmost panel.

This can be contrasted with the evolution shown in Figure 6, which uses the same parameters as in Figure 5

except for the volume dependence of the dislocation viscosity, which is introduced by setting $p_J = -33 \approx \ln(10)/(J_2 - J_1)$ in order to facilitate a tenfold increase in viscosity when transitioning from the upper to the lower mantle. This results in a significantly different slab shape, *i.e.*, stagnation, which prolongs the duration of the evolution and allows diffusion to become active. Consequently, the fluid content in the descending slab fully diffuses into the surrounding rock.

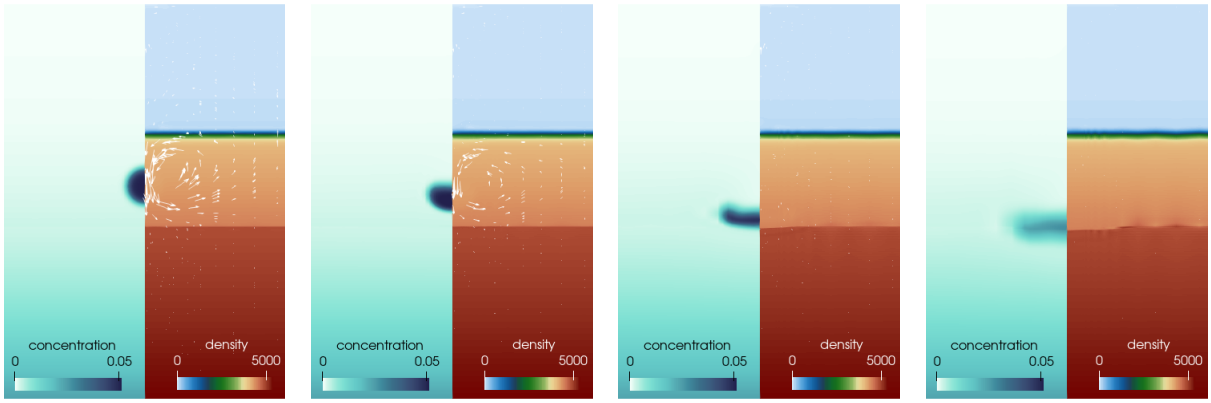

Figure 6: A descenting drop-like slab stagnating on the bottom of the upper mantle and dehydrating there, depicted at four selected time instants. The viscosity in the lower mantle is higher about $10\times$ than in the upper mantle due to choosing $p_J = -33$ in $f_{\rm visc}(J)$ used in (60).

The examples presented above demonstrate that a compressible flow model with non-Newtonian rheology provides a flexible and energetically consistent framework for modelling fluid transport across both the upper and lower mantle in different parameter regimes. By incorporating stored energies in a piecewise C^1 fashion, we can include typical phase transitions directly into the equation of state. The resulting model naturally couples sharp spatial changes in the thermodynamic consistent manner without requiring ad hoc parametrizations. The use of a shear-thinning, non-Newtonian rheology distinguishing shear and bulk viscosities further enhances the model capability to achieve realistic flow fields while preserving thermodynamic consistency. Importantly, the resulting system remains amenable to robust and efficient numerical discretization, enabling long-term simulations over geodynamic time scales. This approach therefore offers a unifying and computationally tractable strategy for simulating complex multiphase mantle dynamics with strong coupling between fluid content, deformation, and material transitions via indicator functions or phase fields.

References

[1] R. Agrusta, S. Goes, and J. van Hunen. Subducting-slab transition-zone interaction: Stagnation, penetration and mode switches. *Earth & Planet. Sci. Letters*, 464:10–23, 2017.

[2] D. Arcay, E. Tric, and M.-P. Doin. Numerical simulations of subduction zones - effect of slab dehydration on the mantle wedge dynamics. *Phys. Earth & Planetary Interiors*, 149:133–153, 2005.

[3] A.Y. Babeyko and S.V. Sobolev. High-resolution numerical modeling of stress distribution in visco-elasto-plastic subducting slabs. *Lithos*, 103:205–216, 2008.

[4] A.N. Beris and B.J. Edwards. *Thermodynamics of Flowing Systems: with Internal Microstructure*. Oxford University Press, 1994.

[5] M.I. Billen. Modeling the dynamics of subducting slabs. *Annu. Rev. Earth Planet. Sci.*, 36:325–356, 2008.

[6] S.A. Chester, C.V. Di Leo, and L. Anand. A finite element implementation of a coupled diffusion-deformation theory for elastomeric gels. *Intl. J. Solids & Structures*, 52:1–18, 2015.

[7] H. Čížková and C.R. Bina. Effects of mantle and subduction-interface rheologies on slab stagnation and trench rollback. *Earth & Planetary Sci. Letters*, 379:95–103, 2013.

[8] H. Čížková, A.P. van den Berg, W. Spakman, and C. Matyska. The viscosity of Earth's lower mantle inferred from sinking speed of subducted lithosphere. *Phys. Earth & Planetary Interiors*, 200–201:56–62, 2012.

[9] H. Čížková, J. van Hunen, A.P. van den Berg, and N.J. Vlaar. The inluence of rheological weakening and yield stress on the interaction of slabs with the 670 km discontinuity. *Earth Planetary Sci. Letters*, 199:447–457, 2002.

[10] F Crameri, H Schmeling, GJ Golabek, T Duretz, R Orendt, SJH Buiter, DA May, BJP Kaus, TV Gerya, and PJ Tackley. A comparison of numerical surface topography calculations in geodynamic modelling: an evaluation of the 'sticky air' method. *Geophysical Journal International*, 189(1):38–54, 2012.

[11] A.M. Dziewonski and D.L. Anderson. Preliminary reference Earth model. *Phys. Earth Planetary Interiors*, 25:297–356, 1981.

[12] M. Faccenda and L. Dal Zilio. The role of solid–solid phase transitions in mantle convection. *Lithos*, 268–271:198–224, 2017.

[13] R. Fischer and T. Gerya. Early Earth plume-lid tectonics: A high-resolution 3D numerical modelling approach. *J. Geodynam.*, 100:198–214, 2016.

[14] E. Fried and M.E. Gurtin. Tractions, balances, and boundary conditions for nonsimple materials with application to liquid flow at small-lenght scales. *Arch. Ration. Mech. Anal.*, 182:513–554, 2006.

[15] A.E. Green and R.S. Rivlin. Multipolar continuum mechanics. *Arch. Rat. Mech. Anal.*, 17:113–147, 1964.

[16] M.E. Gurtin, E. Fried, and L. Anand. *The Mechanics and Thermodynamics of Continua*. Cambridge Univ. Press, New York, 2010.

[17] T.J. Healey and S. Krömer. Injective weak solutions in second-gradient nonlinear elasticity. *ESAIM: Control, Optim. & Cal. Var.*, 15:863–871, 2009.

[18] G.T. Jarvis and D.P. McKenzie. Convection in a compressible fluid with infinite Prandtl number. *J. Fluid Mech.*, 96:515–583, 1980.

[19] M. Kružík and T. Roubíček. *Mathematical Methods in Continuum Mechanics of Solids*. Springer, Cham, Switzerland, 2019.

[20] R. Li et al. How phase transitions impact changes in mantle convection style throughout Earth's history: From stalled plumes to surface dynamics. *Geochemistry, Geophysics, Geosystems*, 26:Art.no.e2024GC011600, 2025.

[21] A. Logg, K.-A. Mardal, and G. Wells (Eds.). *Automated solution of differential equations by the finite element method: The FEniCS book*. Springer, Heidelberg, 2012.

[22] Z. Martinec. *Principles of Continuum Mechanics*. Birkhäuser/Springer, Switzerland, 2019.

[23] A. Mielke and T. Roubíček. A general thermodynamical model for finitely-strained continuum with inelasticity and diffusion, its GENERIC derivation in Eulerian formulation, and some application. *Zeitschr. f. angew. Math. u. Phys.*, 76:Art.no.11 (28pp), 2025.

[24] P.B. Mucha and M. Pokorný. On a new approach to the issue of existence and regularity for the steady compressible Navier-Stokes equations. *Nonlinearity*, 19(8):1747–1768, 2006.

[25] J. Nečas. Theory of multipolar fluids. In L. Jentsch and F. Tröltzsch, editors, *Problems and Methods in Mathematical Physics*, pages 111–119, Wiesbaden, 1994. Vieweg+Teubner.

[26] J. Nečas and M. Šilhavý. Multipolar viscous fluids. *Quarterly App. Math.*, 49:247–265, 1991.

[27] Dirk Peschka, Marita Thomas, and Andrea Zafferi. Reference map approach to eulerian thermomechanics using generic. In *Advances in Continuum Physics: In Memoriam Wolfgang Dreyer*, pages 39–70. Springer, 2025.

[28] G. Ranalli. Mantle rheology: radial and lateral viscosity variations inferred from microphysical creep laws. *J. Geodynamics*, 32:425–444, 2001.

[29] T. Roubíček. Thermodynamics of viscoelastic solids, its Eulerian formulation, and existence of weak solutions. *Zeitschrift f. angew. Math. Phys.*, 75:Art.no.51, 2024.

[30] T. Roubíček. A few notes about viscoplastic rheologies. *arXiv:2506.16785*, 2025.

[31] T. Roubíček. Time discretization in visco-elastodynamics at large displacements and strains in the Eulerian frame. *Math. Mech. Solids*, 30:2365–2401, 2025.

[32] T. Roubíček and U. Stefanelli. Viscoelastodynamics of swelling porous solids at large strains by an Eulerian approach. *SIAM J. Math. Anal.*, 55:2475–2876, 2023.

[33] N. Suenaga, Y. Ji, S. Yoshioka, and D. Feng. Subduction thermal regime, slab dehydration, and seismicity distribution beneath Hikurangi based on 3-D simulations. *J. Geophys. Res.: Solid Earth*, 123:3080–3097, 2018.

[34] P.J. Tackley. Modelling compressible mantle convection with large viscosity contrasts in a three-dimensional spherical shell using the yin-yang grid. *Phys. Earth & Planetary Interiors*, 171:7–18, 2008.

[35] N. Tosi and D.A. Yuen. Bent-shaped plumes and horizontal channel flow beneath the 660 km discontinuity. *Earth & Planetary Sci. Lett.*, 312:348–359, 2011.

[36] V. Turino and A.F. Holt. Spatio-temporal variability in slab temperature within dynamic 3-D subduction models. *Geophys. J. Int.*, 236:1484–1498, 2024.

[37] W.J.M. van Oosterhout and M. Liero. Finite-strain poro-visco-elasticity with degenerate mobility. *Zeitsch. Angew. Math. Mech.*, 104:Art.no.e202300486, 2024.

[38] E. Zatorska. Analysis of semidiscretization of the compressible Navier-Stokes equations. *J. Math. Anal. Appl.*, 386:559–580, 2012.